Interpretable machine learning model for autogenous shrinkage prediction of low-carbon cementitious materials

Benoit Hilloulin, van Quan Tran

Interpretable Machine Learning Model for Autogenous Shrinkage Prediction of Low-Carbon Cementitious Materials

Benoît Hilloulin[1],Van Quan Tran[2,] *

[1] Nantes Université, Ecole Centrale Nantes, CNRS, GeM, UMR 6183, F-44000 Nantes, France – e-mail: benoit.hilloulin@ec-nantes.fr

[2]University of Transport Technology, Hanoi 100000, Vietnam

*Corresponding author: quantv@utt.edu.vn

Highlights

- A large database about the autogenous shrinkage of concrete with SCM is built
- Ensemble machine learning models can predict the autogenous shrinkage efficiently
- ML models can perform better than B4 and CEB models modified versions.
- SCM influence can be interpreted using SHAP analysis
- Insights into blended cement concrete shrinkage behavior can be envisioned.

Abstract

Supplementary cementitious materials (SCM) are key components of low-carbon cementitious materials. However, their effects, especially for the emerging high cement replacement ratio formulations, are sometimes very challenging to predict, leading to restrictions in most standards. Through advanced Machine Learning techniques, this study provides novel insights into the autogenous shrinkage properties of concrete containing various kinds of supplementary cementitious materials such as slag, fly ash, silica fume, calcined clay, and filler. Four machine learning models are optimized and their predictions are compared on a dedicated database, including ternary and quaternary cement blends. The Extreme Gradient Boosting (XGBoost) model exhibited the highest accuracy among these models. Interpretative tools such as SHAP analysis are then used to obtain novel information about the relative influence of the SCM on the autogenous shrinkage depending on their dosage. The model is finally compared to the recently modified versions of the B4 and the CEB analytical models to predict the autogenous shrinkage of unknown concrete formulations. The model showed significantly better predictions than the analytical models, and a web application is proposed, paving the way for precise and

interpretable autogenous shrinkage predictions of cementitious materials incorporating SCM.

Keywords: Concrete; Autogenous Shrinkage; Supplementary Cementitious Material (SCM); Machine Learning; XGBoost; Shrinkage Models.

1 Introduction

Decreasing cementitious materials' carbon footprint is necessary to limit the overall environmental impact of the construction industry. This decrease can be achieved through several techniques such as the construction and demolition waste (CDW) usage, for example, the use of crushed concrete waste into Recycled Aggregate Concrete (RAC) [1], or the extensive use of supplementary cementitious materials, some of them being industrial byproducts [2–4]. However, these additions considerably impact the behavior of cementitious materials, and, because of these rapid evolutions, such novel components are rarely very well understood nor precisely considered in the construction standards. More specifically, it is generally admitted that concrete early age deformations can induce severe structural evolutions. Apart from environmental degradations, these deformations are mostly due to shrinkage and creep mechanisms [5]. For example, high-performance and ultra-high performance concrete (HPC and UHPC) exhibit significant early age deformations because of their low water-to-cement ratio. Indeed, while deformation of normal strength concrete is primarily governed by drying shrinkage, which occurs some weeks or months after setting due to a water loss, deformation in low water-to-cement concrete can develop very quickly at an early age because of the rapid evaporation of water from the surface of the specimen, namely plastic shrinkage, or because of the consumption of water during the hydration directly causing chemical shrinkage, and generating capillary depressions leading to macroscopic deformations referred to as autogenous shrinkage. It has been found that autogenous shrinkage can represent more than half of the total deformation in ultra-high performance concrete [6], creating considerable stresses at a microscale that can lead to cracking. As cracking should generally be avoided, either because of structural concerns or aesthetic reasons[7,8], specific attention should be paid to early-age deformation of low water-to-cement ratio high and ultra-high performance concrete.

Several analytical models have been introduced during the last decades to predict shrinkage. The major construction codes provide quick ways to estimate the shrinkage amplitude of several

concrete mixes based on their composition and, in some cases, by considering standard strength characteristics such as the 28-days compressive strength. Power and exponential laws have been introduced to describe the shrinkage amplitude evolution relatively to time [9,10]. Thanks to these laws, the quick increase in autogenous shrinkage amplitude during the first weeks can be grasped. Most of these models are a combination between empirical laws and advanced theories. For example, B4 model [10] is supported by the solidification theory, the theory of microprestress relaxation, activation energy concepts, the moisture diffusion theory, and damage models for microcracking, and proved very good results in predicting autogenous and drying shrinkage of structural elements [11]. Other models have been proposed in reference codes such as Eurocode 2, fib CEB MC 10 [9,12,13]. Recent improvements of both the B4 and the CEB MC 10 model have been proposed to take into consideration the influence of some supplementary cementitious materials [14,15]. These models have been found particularly effective in predicting long-term predictions deformation of concrete, but several shortcomings have been noticed concerning early-age prediction and regarding actual concrete formulations, which can include a high proportion of additions [15,16]. Moreover, the growing use of various supplementary cementitious materials (SCM), leading to ternary or quaternary concrete mixes is which synergistic effects may arise, is rarely taken into consideration.

Indeed, due to economic and environmental considerations, an increasing amount of SCM is being used in recent concrete formulations. Various SCM such as calcined clay, fly ash, ground granulated blast furnace slag, later referred to as slag, and silica fume commonly replace cement, while additions like fillers may partially replace cement or only play a physical role in increasing the overall compacity of the mix. These additions influence shrinkage mechanisms to various extents, especially autogenous shrinkage. It is commonly admitted that silica fume, commonly used in UHPC due to its filling properties and high pozzolanic activity, increases shrinkage even for small replacement ratios [5]. Conversely, fly ash alone has been reported to decrease shrinkage in most studies because of the slower hydration reaction [17,18]. In most published studies, slag increased autogenous shrinkage, especially long-term autogenous shrinkage, because its fineness leads to high reactivity and higher chemical shrinkage than pure cement concrete [19–22]. Some uncertainty remains concerning the influence of slag on the autogenous shrinkage of UHPC since it has been reported that the addition of slag increased the autogenous shrinkage in some cases [15]. With the demand for low-cement concrete, calcined clay, which is readily available around the globe, has been proved to be an interesting product to cut CO_2 emissions due to concrete

formulation. Though calcined clay, generally associated with limestone to produce LC^3 cement, induces novel chemical reactions during hydration, and leads to a fine porosity [23], its influence on the autogenous shrinkage is rarely reported and might not be prejudicial [24–26]. Finally, fillers have been found to decrease shrinkage as they act like small aggregates restricting deformations [27,28], but their interactions with other additions are often only considered from a chemical point of view and are rarely addressed from a shrinkage point of view [27,29].

Therefore, with the increasing complexity of concrete formulations, a better understanding of fundamental evolutions such as autogenous shrinkage is needed. Recent studies have proposed adaptation to the aforementioned analytical models to consider the use of SCM and their eventual combination [15,30]. In [15], CEB Model Code 2010 has been improved by introducing correction factors using an extensive experimental campaign. However, such parameters might not represent other concrete formulation behaviors, and more extensive shrinkage databases should be built.

Recent developments in Machine Learning (ML) have provided novel insights into concrete properties-related issues [31]. Since the publication of the first Artificial Neural Network model (ANN) to predict concrete compressive strength [32], numerous research works have been published to predict concrete compressive strength with ML-based models [33–36]. ML-based models have also proved their interest in predicting other concrete properties such as fresh properties [37], creep [38,39], chloride [40], carbonation resistance [41], frost resistance [42] and shrinkage [43,44]. They can also be used for microscale properties determination and enhancement, such as during indentation [45,46], image analysis [47–50], or large-scale structural monitoring [51,52]. While ML models might have initially appeared as black-box models, recent advances such as features analysis and dubbed SHapley Additives exPlanations (SHAP) introduced novel ways to explore the impacts of the model inputs on the final predictions [53]. Such tools have been used recently in several studies related to concrete [44,54] and might help build advanced autogenous shrinkage prediction models comparable to the existing most performant analytical models such as B4 and CEB models.

This study develops an interpretable ensemble ML model to predict the autogenous shrinkage evolution in low-carbon cementitious materials with SCM. An extensive dedicated database is built, including ternary and quaternary formulations, and optimized ML models are compared to the classic and improved versions of B4 and CEB Model Code models using interpretative tools such as SHAP. Then, a web application is proposed to provide fast and precise shrinkage

predictions to the Civil Engineering community. The manuscript is structured as follows: a first section describes the new shrinkage database developed during this study, then a section presents the numerical methods employed before analyzing and discussing the results and a conclusion.

2 Autogenous Shrinkage Database description and analysis

To develop an accurate model for autogenous shrinkage prediction of concrete incorporating SCM, a comprehensive experimental database is required. To this end, we adopted the method published in [44]. The original NU database containing various creep and shrinkage evolutions of cementitious materials has been extended by low water-to-cement ratio cement paste, mortar or concrete samples autogenous shrinkage curves. This database has been further extended to include more autogenous shrinkage data of various concrete of binary, ternary or quaternary formulations from various sources [15,26,55–60]. In total, a database comprising 347 autogenous shrinkage observations and 28d compressive strength of various concrete mixes has been built. To the authors knowledge, this is the most comprehensive autogenous shrinkage database to date. The final database covers a wide range of water-to-cement and water-to-binder ratios (from normal strength to ultra-high strength concrete) as well as a wide variety of binary, ternary and quaternary formulations. These shrinkage curves were interpolated to obtain 1d, 2d, 7d, 14d, and 28d shrinkage values. Twelve input variables have been considered: water-cement ratio (W/C), water-binder ratio (W/B), aggregate-cement ratio (A/C), cement content (kg/m^3), silica fume content (% cement mass), fly ash content (% cement mass), slag content (% cement mass), calcined clay content (% cement mass) (denoted as metakaolin content), filler content (kg/m^3), amount of superplasticizer (% cement mass), time since the beginning of shrinkage measurements (days) and 28-d compressive strength (MPa). After removing data points with missing data, a database with 1482 datapoints ha been finally obtained. The descriptions and statistical attributes of the input variables are given in Table 1, and Fig. 1 displays their statistical distributions. It can be seen that a wide range of compositions has been investigated as water-to-binder ratios range from 0.16 to 0.86, cement content ranges from 167.4 kg/m^3 to 1632 kg/m^3 (cement paste) with a large proportion of values between 167 kg/m^3 and 700 kg/m^3 for concretes. Supplementary cementitious materials contents reflect the actual wide variety of formulations, some of them with important substitution amounts. Indeed silica fume content, fly ash content, slag content, calcined clay and filler content up to 50%, 150%, 400%, 57.4% and 125% relatively to cement mass were

considered. A maximum shrinkage value of around -2089 με has been obtained and a median shrinkage value of -114.7 με can be calculated. Common autogenous shrinkage features can be retrieved from the 2D scatter plots exposed in Fig. 1 by plotting linear regressions: shrinkage increases with smaller W/B and A/C values, while it generally increases with higher cement or silica fume content as well as higher compressive strength as they are generally associated to low W/B values.

Correlations between the model parameters were calculated too. Fig. 2 gives a graphical representation of the correlation matrix. As expected, strong positive correlations can be observed between, W/B, A/C and shrinkage, and strong negative correlations can be observed between shrinkage and fc28, cement content or silica fume content. However, no strong correlations between input variables, and as such, all these variables were used as the input for ML.

Table 1. Description of the database used in this study

	Unit	Min	Q25%	Mean	Median	$Q_{75\%}$	Max	Std	Skw
W/C	-	0.180	0.320	0.444	0.390	0.500	1.600	0.188	2.807
W/B	-	0.160	0.290	0.360	0.336	0.400	0.860	0.117	1.295
A/C	-	0.00	3.28	3.90	3.90	4.73	11.56	1.77	0.36
Cement content	kg/m^3	167.4	360.0	472.1	440.0	496.0	1632.0	222.3	2.9
Silica fume content	% cem	0.0	0.0	3.0	0.0	0.0	50.0	7.2	3.7
Fly Ash	% cem	0.0	0.0	8.2	0.0	0.0	150.0	18.3	3.1
Slag content	% cem	0.0	0.0	9.8	0.0	0.0	400.0	40.6	6.7
Metakaolin content	% cem	0.0	0.0	1.6	0.0	0.0	57.4	8.2	5.7
Filler content	% cem	0.0	0.0	4.7	0.0	0.0	125.0	14.5	4.1
Superplasticizer content	% cem	0.0	0.0	1.5	0.8	1.8	11.8	2.2	2.3
Compressive strength fc28	MPa	16.5	45.9	67.1	63.0	85.7	162.0	29.4	0.8
Time of measurement	days	1.0	2.0	9.7	7.0	14.0	28.0	9.6	1.0
Shrinkage/Swelling	μm	-2089.600	-243.000	-182.832	-114.700	-28.650	78.900	237.617	-2.576

Skw=Skewness; Std=Standard deviation;

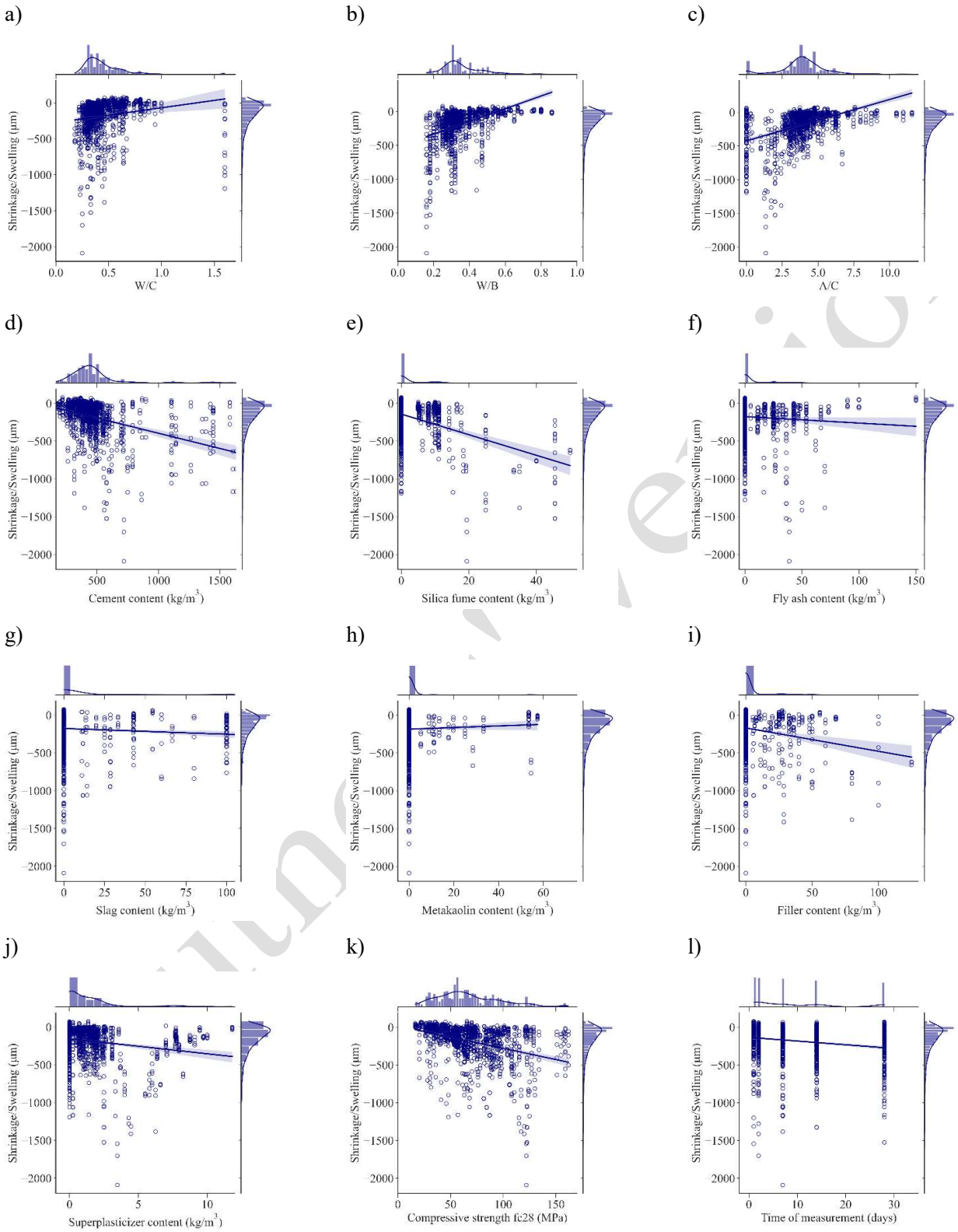

170 **Fig. 1.** Data distribution of each input variable and the output variable (shrinkage/swelling).

171

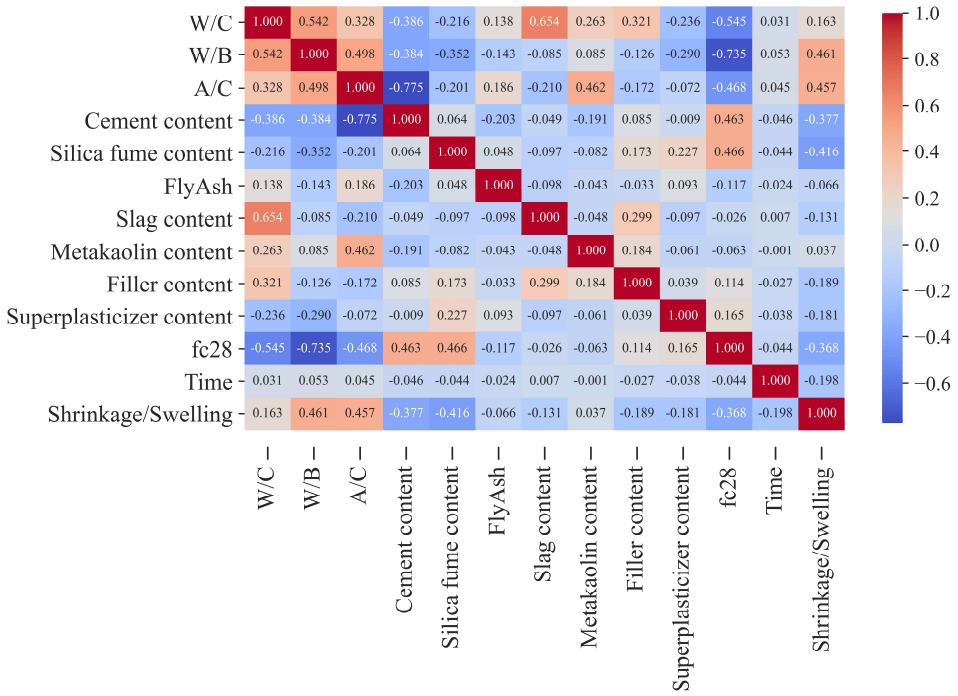

Fig. 2. Pearson correlation of all feature and Shrinkage/Swelling

3 Shrinkage prediction using Machine Learning and Analytical models

3.1 Modeling strategy

The modeling strategy is four steps presented in Figure 3:

- Step 1: Collection a database consisting 12 input variables and one output variable "shrinkage/swelling".
- Step 2: Determination the best performance of ML model

All the observation data from the original database have been classically split into training and testing datasets. 70% of whole dataset is used to building the four ML models including SVM, ANN, GB and XGB with aided of metaheuristic optimization algorithm Simulated Annealing (SA) Optimization algorithm which tunes the hyperparameters of four ML algorithms. The K-Fold Cross Validation (CV) is integrated in the tuning hyperparameter process for validating the cost function R^2 of optimization process. The evaluation ML performances are carried out with aided of three metrics, such as R^2, RMSE and MAE, in prediction of Shrinkage/Swelling. Based on the best performance, the best ML model is proposed for the next steps.

- Step 3: Interpretation of XGB black box with SHAP value

  In this step, the SHAPley Additive exPlanations (SHAP) [61] based on the best ML model is used for the interpretation of predicted Shrinkage/swelling values. The effect of each feature is quantified by SHAP global and SHAP local.

- Step 4: Comparison of predicted value based on the best ML model with B4 and CEB analytical models

  The concrete formulations in the original database have been divided into a training and a test set to guarantee that no shrinkage value from any concrete with all time of measurement in the test set is known. Then the best Machine Learning model is fitted on this training set, and its performance is compared to the performance of the analytical models on the test set.

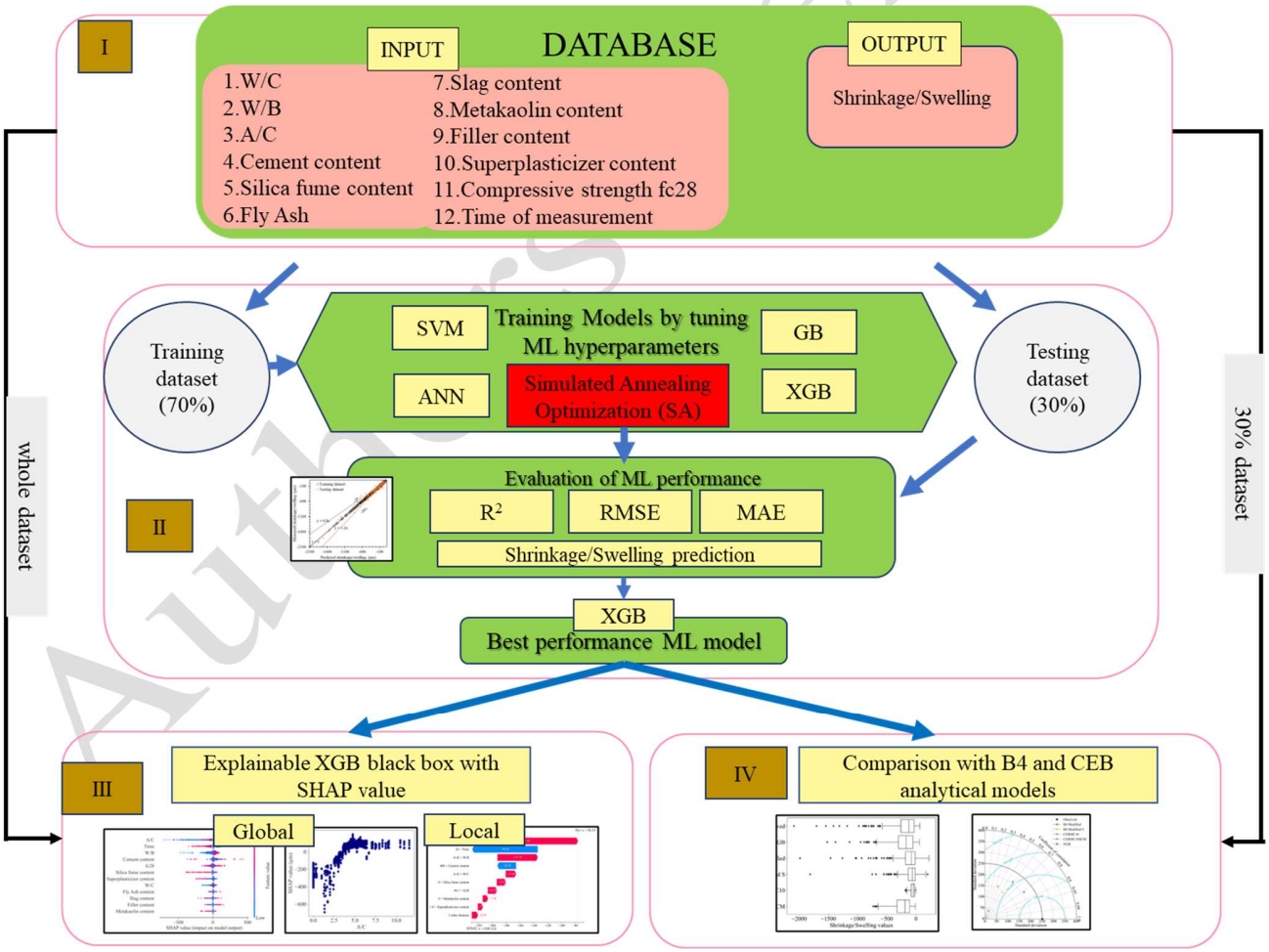

Fig 3. Conception of shrinkage/swelling investigation

3.2 Machine learning models

3.2.1 Support Vector Machine (SVM)

The support vector machine algorithm introduced by Vapnik [62] can be used to address classification difficulties. For the solution of regression and prediction issues, the support vector machine was further modified and dubbed support vector machine regression (SVR) [63]. The SVR method sought to reduce the generalization error and get the best solution using the structural risk minimization concept. The Gaussian radial basis function was used in this work to transition from a lower-dimensional feature space to a higher one, allowing for linear regression and improved fitting of the training dataset. The following linear function can be used to represent the output variable:

$$f(x) = \langle \omega \cdot \varphi(x) \rangle + b \tag{1}$$

where $\langle \cdot \rangle$ denotes the dot function; $\varphi(x)$ is a transformation that translates the input feature to a higher dimensional feature space; b is the function's parameter vector (model bias); ω are the minimum values derived from the following equation:

$$minimise \left[\frac{1}{2} \|\omega\|^2 + C \sum_{j-i}^{n} (\xi_j + \xi_j^*) \right] \tag{2}$$

$$considering \begin{cases} y_j - \omega \cdot \varphi(x_j) - b \leq \varepsilon + \xi_j \\ \omega \cdot \varphi(x_j) + b - y_j \leq \varepsilon + \xi_j^* \\ \xi_j, \xi_j^* \geq 0 \end{cases} \tag{3}$$

where ξ_j, ξ_j^* are the slack variables; C is the regularization parameter; ε is the insensitive loss function (error between the test and forecast values); y_j is the test result; and n is the sample size.

3.2.2 Artificial Neural Network (ANN)

The most widely used machine learning model is ANN, which is based on biological neural networks. It is made up of input neurons (similar to synapses), multiplied by weights representing the intensities of the relevant impulses, and then determined by the neuron's activation function. Finally, the required result will be computed by another function (perhaps an identity function). It is feasible to acquire the output matching to certain inputs by altering the weight of the artificial neuron. However, when there are too many neurons, calculating these weights becomes problematic. At this time, numerous ways are being developed to modify the weights of the neurons in order to get the output as rapidly as feasible. In this study, the solver for weight optimization contains three methods including 'LBFGS' Limited-Memory Broyden-Fletcher-Goldfarb-Shanno method of quasi-Newton methods, 'SGD' refers to stochastic gradient descent and the last 'ADAM' referring

to a Stochastic Gradient-Based Optimizer proposed by Kingma et al. [64]. In this investigation, the best optimization solver will be selected by the metaheuristic algorithm in the process of tuning hyperparameters.

3.2.3 Gradient Boosting (GB)

Gradient Boosting (GB) improves predictions by using a method called as augmentation. The algorithm in boosting attempts to examine and correct predictions that are not acceptable on the first iteration [65]. The algorithm's iterative process for correction then continues until the desired prediction is obtained. Increased assistance for decreasing bias and variation in order to strengthen poor learners.

Gradient Boosting is the process of combining several weak predictive models into a single strong model [66]. In this case, a poor prediction model may perform somewhat better than random guesses.

The model using the Boosting ensemble learning strategy can be expressed as follows:

$$F_N(x) = \sum_{n=1}^{M} \alpha_n f_n(x) \tag{4}$$

The ensemble learning model $F_N(x)$ is generated by the linear combination of N basic learning machine models, where $f_n(x)$ represents the mth basic learning machine and n represents the weight of the nth basic learning machine.

The gradient boosting algorithm operates on the gradient descent approach, which is based on the functional. To begin, the goal function is as follows:

$$E = \sum_{t=1}^{T} L\left(y_t, F_N(x_t)\right) = \sum_{t=1}^{T} L\left(y_t, \alpha_n \times f_n(x_t)\right) \tag{5}$$

The number of samples is T, the number of basic learning machines is N, and the loss function is L. The training procedure is to train each basic learning machine fn, n-1, 2,..., N in turn so that the objective function value E is the smallest, that is, the training outcomes for the nth basic learning machine are as follows.

$$\sum_{t=1}^{T} L\left(y_t, F_{n-1}(x_t) + \alpha_n \times f_n(x_t)\right) \cong \sum_{t=1}^{T} L\left(y_t, F_{n-1}(x_t) + \sum_{t=1}^{T} \frac{\partial L}{\partial F_{n-1}(x_t)} \times f_n(x_t)\right) \tag{6}$$

According to the principle of gradient descent, the optimal model should be the negative gradient direction of the objective function, that is:

$$f_n^*(x) = \arg\min_{f,\alpha} \sum_{t=1}^{T} L\left(-\frac{\partial L}{\partial F_{n-1}(x_t)} - \alpha \times f(x_t) \right)^2 \quad (7)$$

After obtaining the best A, coefficient S can be found by minimizing the objective function, namely:

$$\alpha_n^* = \arg\min_{\alpha_n} \sum_{t=1}^{T} L\left(y_t, F_{n-1}(x_t) + \alpha_n \times f_n^*(x_t) \right) \quad (8)$$

The preceding steps are repeated until all N basic learning machines and coefficients have been trained, and a learning model based on Equation 1 has been generated. The gradient boosting approach is used in the learning model, and the next fundamental machine learning model may further increase the accuracy based on the previous underlying machine learning models, reducing the model's deviation. This is the distinction with the Bagging. Basic machine learning can be a low-accuracy model; through the improvement approach, the accuracy of the entire model can be steadily increased, but there is a certain degree of fit at the same time.

3.2.4 Extreme Gradient Boosting (XGB)

The Extreme Gradient Boosting (XGB) algorithm is a cutting-edge method for solving supervised learning problems with high precision [26]. If Deep Learning only accepts raw data in numerical form (which must typically be converted to n-vectors in the real number space), XGB accepts tabular datasets of any size, including categorical data. Furthermore, XGB has a rapid training speed, can scale for parallel computing on several servers, and can be GPU-accelerated, therefore Big Data is not an issue for this model. The earliest and most well-known model of the most recent generation of tree booster ensembles is the XGB; a representation of this approach is the Gradient Boosting Decision Tree (GB) or Multiple Additive Regression Tree (MART).

The basic idea behind XGB is to first train a tree with the training set and the real value of the sample (i.e. the standard response), and then use that tree to forecast the training set to acquire the proper value. The residuals are the predicted value of each sample, as well as the difference between the forecast and the real value. The second tree is then trained, but this time instead of using the real number, use the residual as the standard response. After training two trees, the residuals of the sample can be used to train more trees. To stop training, the total number of trees can be selected explicitly or based on particular indicators.

The XGB algorithm can be thought of as a K-tree additive model:

$$\hat{y}_i = \sum_{k=1}^{K} f_k(x_i), f_k \in F \quad (9)$$

The gradient boost model does not learn the weights of the d-dimensional space but directly learns the decision tree set, where F is a function space consisting of all trees (here the regression tree is also a partial function and the varied values of the different portions form a tree). The objective function of XGB is a sum of a particular loss function assessing overall predictions and a sum of all predictors' regularization terms (K trees).

Mathematically:

$$obj(\theta) = \sum_{i}^{n} l(y_i - \hat{y}_i) + \sum_{k=1}^{K} \Omega(f_k) \quad (10)$$

Where *l* is the loss function, which is the difference between the expected and actual outputs $\hat{y}_i$ and y_i. While is a measure of how complicated the model is, it aids in preventing model over-fitting and is determined using:

$$\Omega(f_k) = \gamma T + \frac{1}{2}\lambda \|w\|^2 \quad (11)$$

The number T in the preceding equation reflects the number of leaves on the tree, and w represents the weight of each leaf.

3.2.5 Simulated Annealing Optimization algorithm (SA)

Kirkpatrick et al. [67] pioneered simulated annealing (SA) in 1983. This metaheuristic method is based on physical phenomena seen in continuum mechanics. To avoid becoming stuck in local minima, SA employs a random search engine represented by Markov chains. SA employs solution variants to increase the objective function while still maintaining the solutions, albeit the least efficient, within specified constraints. Any adjustment that improves the objective function, J, is permitted in the minimization problem; however, candidates that raise J are also included in the solution set with probability p, which is known as the transition probability [68]:

$$p = \exp\left[-\frac{\Delta E}{k_B T}\right] \quad (12)$$

where k_B is Boltzmann's constant, T is the annealing process temperature, and E is the energy level, is connected with the goal function modification by the constant, [68].

$$\Delta E = \gamma \Delta J \tag{13}$$

A random threshold, r, such that p > r, determines whether a solution modification is acceptable. T lowers and the system cools down during optimization. A high T indicates a high-energy system that is difficult to reduce, whereas a low T indicates a low-energy system that may be trapped in a local minimum [69]. The proper decision T may be to first search the space for the global minimum and then, as the system cools down, converge to a solution with sufficient accuracy [68]. Stopping conditions, such as limiting the number of repeats or focusing on the improvement of the goal function, are incorporated in t_f [70].

3.2.6 Performance evaluation of models

In order to evaluate the performance of ML models, three popular statistical metrics, such as coefficient of determination R^2, Root Mean Square Error (RMSE), and Mean Absolute Error (MAE), are introduced in following:

$$R^2 = \frac{\sum_{j=1}^{N}(p_{0,j} - \overline{p_0})(p_{t,j} - \overline{p_t})}{\sqrt{\sum_{j=1}^{N}(p_{0,j} - \overline{p_0})^2 \sum_{j=1}^{N}(p_{t,j} - \overline{p_t})^2}} \tag{16}$$

$$\text{RMSE} = \sqrt{\frac{1}{N}\sum_{j=1}^{N}(p_{0,j} - p_{t,j})^2} \tag{17}$$

$$\text{MAE} = \frac{1}{N}\sum_{j=1}^{N}\left|p_{0,j} - p_{t,j}\right| \tag{18}$$

Where $p_{0,j}$ is the shrinkage/expansion value of the i-th sample point in the database; $p_{t,j}$ is the machine learning model prediction value for the i-th sample point; $\overline{p_0}$ is the averaged experimental value of shrinkage/expansion; and $\overline{p_t}$ is the mean predicted value. Both MAE and RMSE explicitly quantify the residual error at each sample point and thus provide an accurate assessment of model performance. R2 normalizes the squared residual error with the database variance and generates dimensionless values ranging from 0 to 1. Because RMSE is often seen to be more understandable because it is equivalent to measured values and handy for comparing the performance of different models, it was chosen as the primary metric index.

3.2.7 K-Fold Cross Validation technique

To tune hyperparameters in machine learning algorithms, K-fold cross-validation (CV) is utilized. Choosing k affects the variance; a low k value results in significant variance or bias. Furthermore, while deciding on k, the data quantity and computational capabilities of the system must be taken into account. The value of k in this study is set to10 [71,72], indicating that the number of training and testing rounds is ten . The dataset is split into two parts: training and testing. The training data area is partitioned into k sections of equal size. The model is then trained with different hyperparameters on k-1 subsets and evaluated on the last subset. The process is repeated k times before averaging the evaluation results as illustrated in Figure 4.

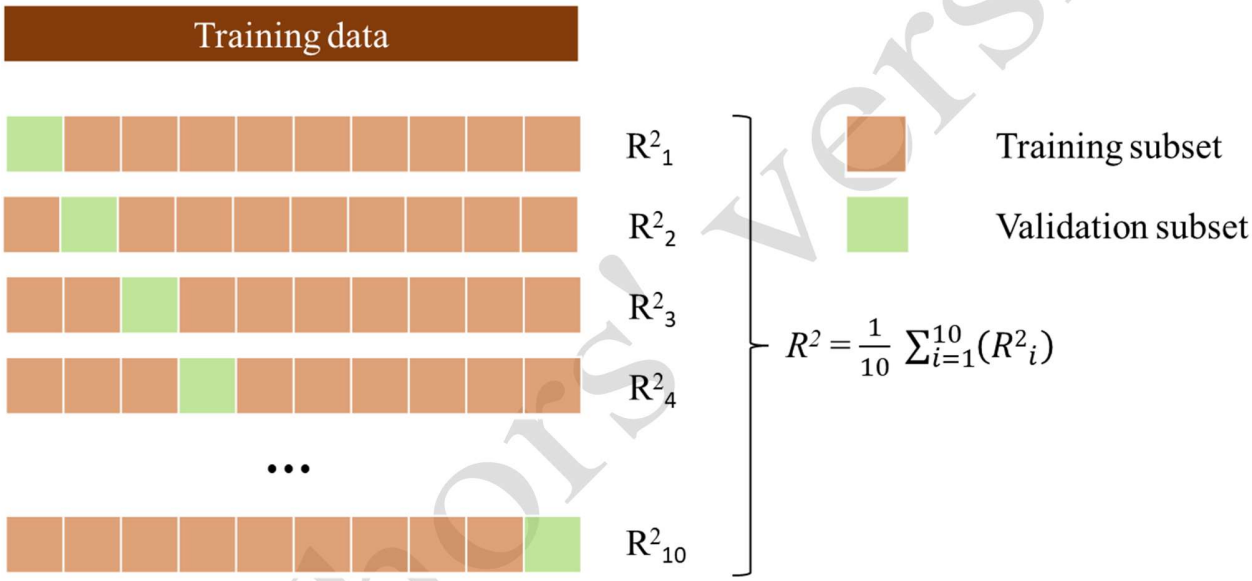

Fig 4. 10-Fold CV of training dataset with cost function of R^2 coefficient of determination

3.3 Comparison with Analytical Models

Three analytical models are also adopted for comparison to examine the prediction accuracy of the machine learning models detailed above. These models are the B4 model [10], CEB MC 10 [9] model and a modified version of CEM MC 10 model to include the effect of SCM which has been introduced recently [15] and will be referred to as 'CEBMC10SCM' model in this study. The autogenous shrinkage model prediction are given as follows:

- Modified B4 model [73]:

Using this composition-based model, the autogenous shrinkage can be calculated at any time:

$$\epsilon_{au}(t) = k_\gamma k_s C t^n \quad (19)$$

where $k_\gamma$depends on the cement type, $k_s = \left\{1 + 3\left(\frac{SiO_2}{Cement}\right)\right\}\left\{1 + 2\left(\frac{Slag}{Cement}\right)\right\}$ takes into account the cement substitution by silica fume or slag, the prefactor C depends on the water-to-cement and aggregate-to-cement ratios : $C = \frac{100}{(w/c)^{2.5} + \left(\frac{a/c}{10}\right)^{1.5}}$ and the exponent factor n, close to 0.2, reads $n = 1.2 - 0.1(a/c) + \left(-0.14 + 0.005(a/c)\right)\ln C$.

- Modified B4 S model [73]:

The autogenous shrinkage value can be calculated using the 28d compressive strength without any information regarding the formulation and reads:

$$\epsilon_{au}(t) = 12 f_c (1 - g)^{1.7} t^{0.2} \quad (20)$$

where f_c is the 28d compressive strength and $g = (volume\ of\ aggregates)/(volume\ of\ concrete)$ (default values of 0.7 and 0.0 can be used for concrete and cement pastes respectively).

- CEB MC 10 model:

$$\epsilon_{cas}(t) = \epsilon_{cas0}(f_{cm}) \cdot \beta_{as}(t) \quad (21)$$

where $\beta_{as}(t) = 1 - \exp\left(-0.2\sqrt{t}\right)$ the time function of autogenous shrinkage and $\epsilon_{cas0}(f_{cm}) = -\alpha_{as}\left(\frac{0.1 f_{cm}}{6 + 0.1 f_{cm}}\right)^{2.5} \cdot 10^{-6}$ the notional autogenous shrinkage coefficient, where α_{as} is a coefficient depending on cement type and f_{cm} is the 28-d compressive strength.

- CEB MC 10 modified for SCM consideration [15]:

$$\epsilon_{cas}(t) = k_{SCM} \cdot \epsilon_{cas0}(f_{cm}) \cdot \beta_{as}(t) \quad (22)$$

where k_{SCM} is a correction factor to included the impact of SCM which, in the case of autogenous shrinkage, reads $k_{SCM} = (1 + 0.24f + 0.4m - 0.35s) \cdot 4M$ where f is the replacement ratio of fly ash (%), m the replacement ratio of calcined clay (%), s the replacement ratio of slag and M the multi-SCM coefficient (binary $M = 0.95$, single $M = 1.0$).

4 Results and Discussion

4.1 Models hyperparameters tuning

The ML model parameters have been tuned using the Simulated Annealing (SA) optimization to obtain the most performant model considering R^2 metric. Surface plots of the R^2 values for several hyperparameter values of the XGB model are reported in Fig. 5. As illustrated in these figures, extended zones of optimized parameter values could be found in most cases. For example, as illustrated in Fig. 5 a), R^2 values higher than 0.91 could be obtained for learning rates lower than 0.5 and more than 500 iterations. A maximum depth of 4 led to the best results as illustrated in Fig. 5 b) while various values of the minimum loss reduction required to make a partition on a leaf node of the tree (min split loss) could generate good results, as illustrated in Fig. 5 c) and d). Based on this optimization analysis carried out by SA, the best hyperparameters values of the four ML models were selected. These values are reported in Table 2.

a)

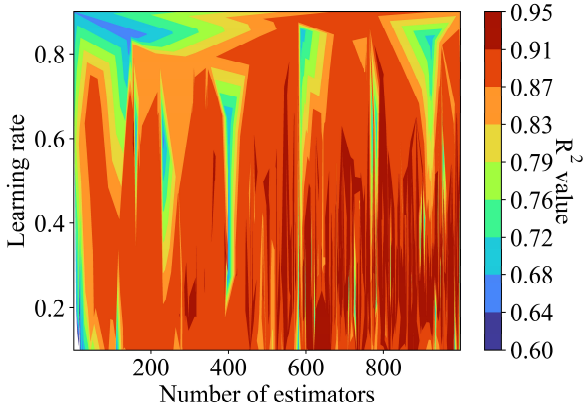

b)

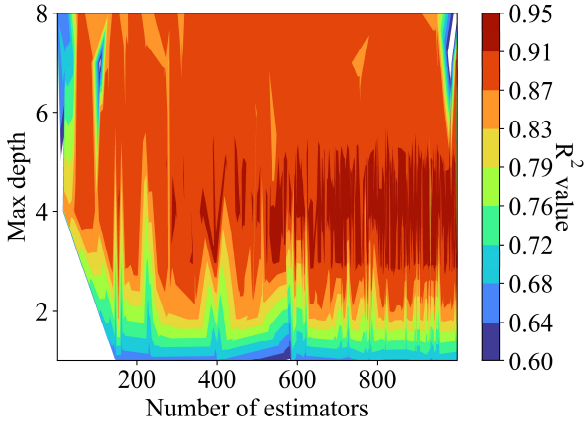

c)

d)

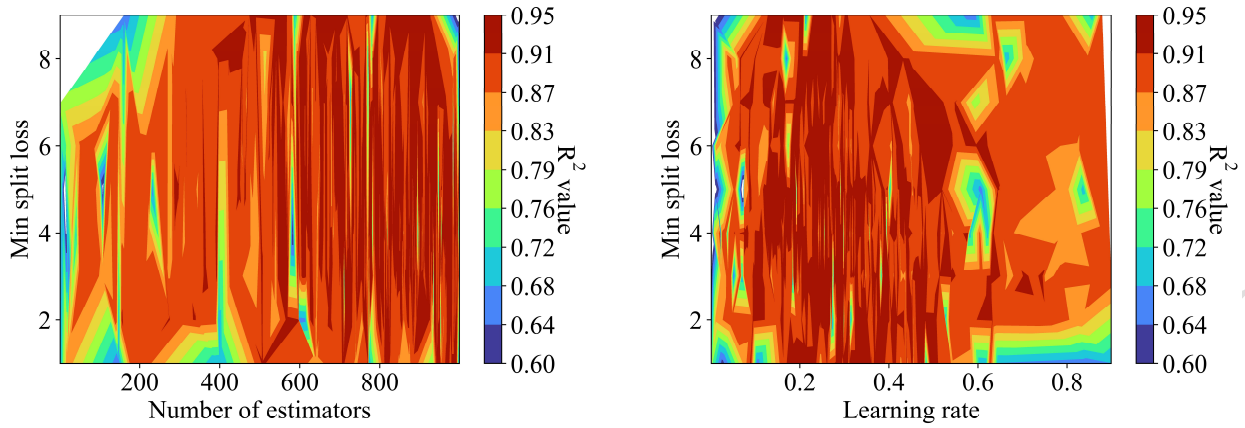

Fig 5. Tuning XGBoost hyperparameters: surface plots of R^2-values using 10-fold cross-validation.

Table 2. Tunned hyperparameters of the ML models.

XGB	Nb of trees 1197	Learning rate 0.6680	Max depth 10	Min split loss 4			**R^2 0.9311**
GB	Nb of trees 887	Learning rate 0.2740	Max depth 10	Max features 10	Min samples split 0.0560	Min samples leaf 0.0580	**R^2 0.9284**
SVM	C 1491	γ 0.3610	ε 0.0610	Kernel RBF			**R^2 0.8089**
ANN	Nb of neurons (19,9)	Activation RELU	Solver LBFGS	Max iteration 4000			**R^2 0.8054**

4.2 Machine learning models typical predictions

The results obtained by the four models on the training and test sets are displayed in Fig. 6. As illustrated in the figure, all models performed well on the training sets with R^2 values higher than 0.94. Most training set predictions fall within the interval between 0.8 times and 1.2 times the measurement shrinkage value, except for very small shrinkage values. However, Gradient Boosting and XGBoost algorithms outperformed SVM and ANN models. The first two models provided high-quality predictions for various shrinkage values, while the latter two models were relatively prone to errors, even for small

shrinkage values. The detailed metrics corresponding to the model results are reported in Table 3. XGB model performed better than the other models, and the R^2 value associated with its prediction of the test set was 0.9733, which corresponds to an RMSE of around 38.9 με.

The mean absolute error (MAE) distribution has been analyzed for the four models, as illustrated in Fig. 7. It can be seen that the MAE remained limited for the XGB model as compared to the SVM and ANN models. Moreover, the maximum MAE measured for the XGB model, close to 200 με was almost twice as small as the maximum MAE obtained by the SVM and the ANN model.

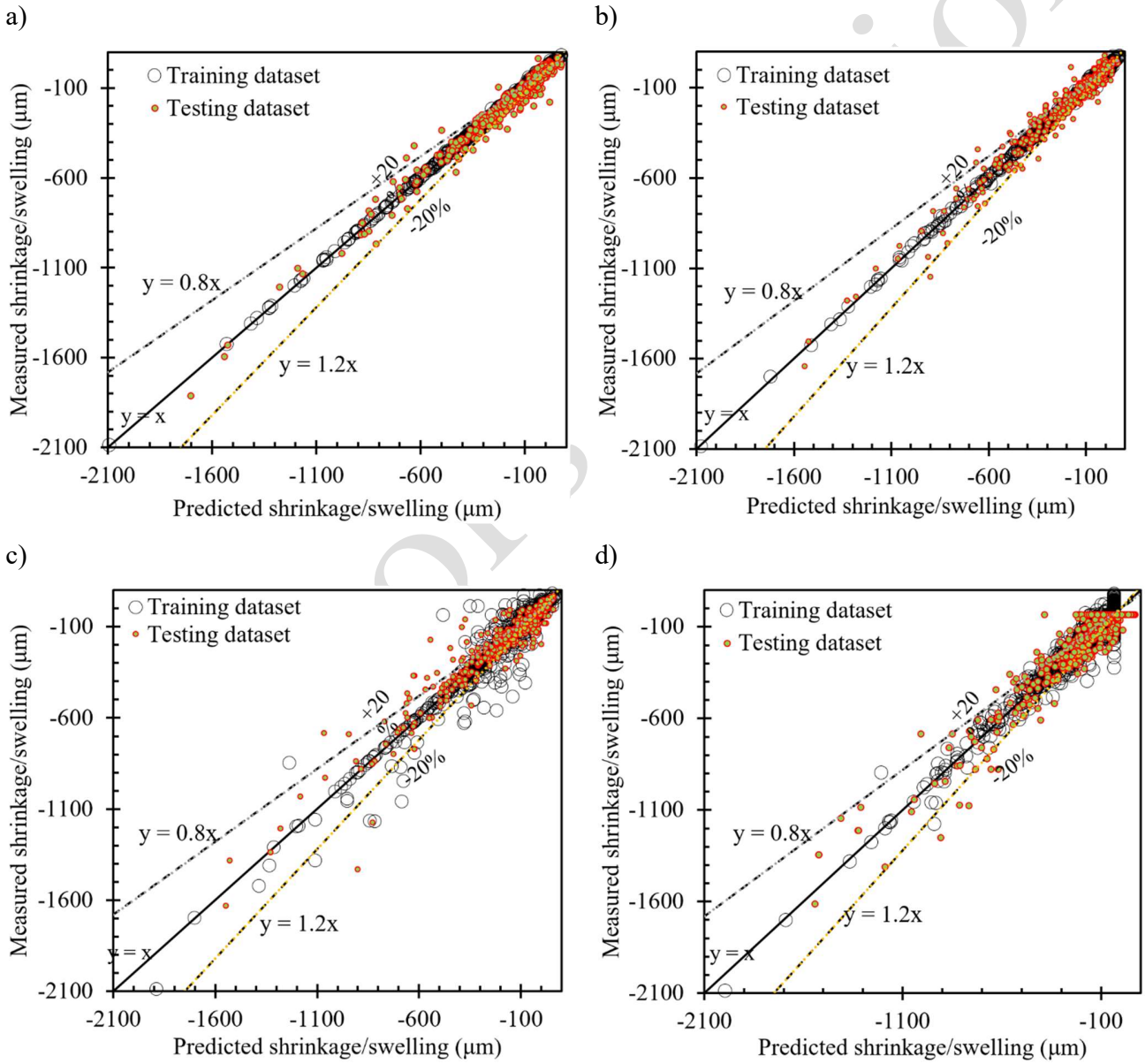

Fig. 6. Shrinkage/Swelling predicted by different ML models: a) XGB, b) GB, c) SVM and d) ANN models

400 **Table 3.** Comparison of machine learning algorithms for autogenous shrinkage prediction of
401 concrete incorporating SCM.

	Train			Test		
	R^2	RMSE (με)	MAE (με)	R^2	RMSE (με)	MAE (με)
XGB	0.999	6.341	3.993	0.973	38.909	25.249
GB	0.998	7.816	4.620	0.965	45.797	31.039
SVM	0.941	57.085	21.974	0.915	71.775	40.764
ANN	0.949	50.695	37.303	0.910	79.288	56.594

402

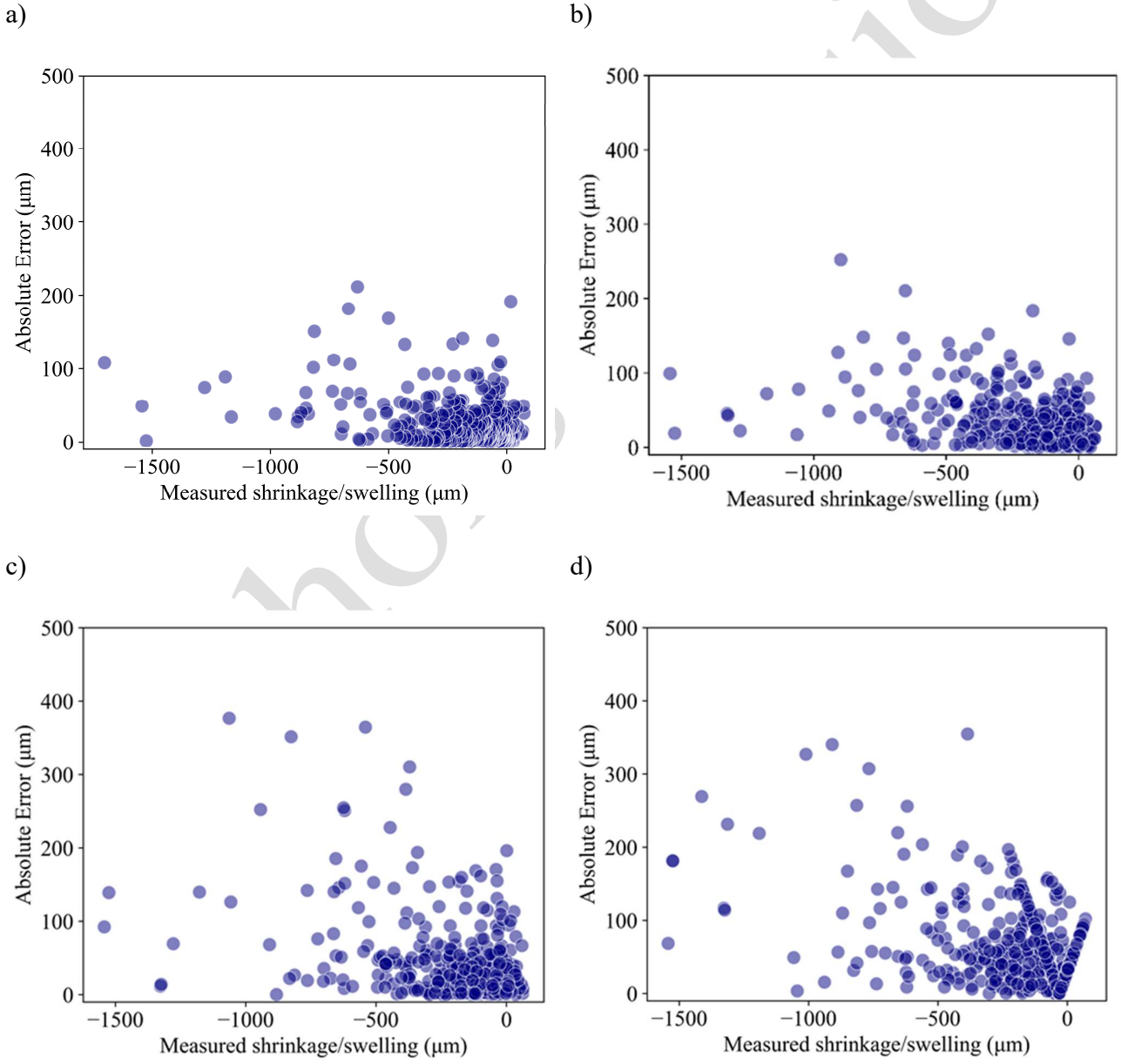

403 **Fig 7.** Distribution of the absolute error: a) XGB, b) GB, c) SVM, and d) ANN models.

4.3 Feature importance and sensitivity analysis

4.3.1 Global interpretation

The most influential features on the shrinkage predictions have been obtained from the model using SHAP. The global SHAP values are reported in Fig. 8, the features classified in descending order based on their influence from top to bottom. The results align with the previous study published by the authors dedicated to autogenous shrinkage prediction of cementitious materials incorporating SAP and SCM even if the database has been largely extended and the model results improved [44]. Indeed, the most influential parameters are the A/C ratio, time, W/B ratio, cement content, the 28d compressive strength, silica fume content, superplasticizer content, W/C ratio, fly ash, slag, filler, and last calcined clay content. The relative influence of the most influential parameters can still be easily determined:

- increasing A/C ratio increases SHAP value, e.g., decrease shrinkage
- increasing time values correspond to higher shrinkage values
- increasing W/B and W/C ratios tend to decrease shrinkage
- high silica fume replacement ratio or cement content predominantly induces higher shrinkage

However, the global influence of the other parameters, mainly SCM other than silica fume, might not be that clear at first sight. Most fly ash highest values are associated with positive SHAP values, which means that a high fly ash content globally decreases shrinkage. Similarly, the highest filler contents are associated with positive SHAP values, i.e., decreased shrinkage. Since the highest calcined clay contents are associated with the most negative SHAP values, its adverse effect on autogenous shrinkage can be confirmed for high replacement ratios. Last, slag and 28d compressive strength effects cannot be analyzed easily from this global perspective. To this end, more detailed insights are needed using the features dependance plots.

SHAP can also give information about the feature dependency of the results, as illustrated in Fig. 9. Indeed, feature dependence plots reveal how the SHAP values change depending on the values of the features. As illustrated in Fig. 9 a), the SHAP values largely increase when the A/C values increase, especially when A/C values increase from around 1.0 to 4.0, corresponding to the transition from mortar to concrete. This increase of around 800 με highlights the relative influence

of the A/C ratio on the autogenous shrinkage phenomenon. For A/C values higher than 4.0, SHAP value is almost constant, meaning there is no interest in further increasing the A/C ratio to reduce the autogenous shrinkage. The water-to-binder ratio's influence can be analyzed using Fig. 9 b). From this figure, it can be seen that the SHAP value increases from the minimum w/b considered in this study, e.g. 0.16, to approximately 0.5. This gradual increase from around -300 με to around 50 με confirms that autogenous shrinkage arises in cementitious materials of W/B ratio smaller than 0.5. However, it is worth noting that the W/B relative influence is around twice as small as the A/C influence.

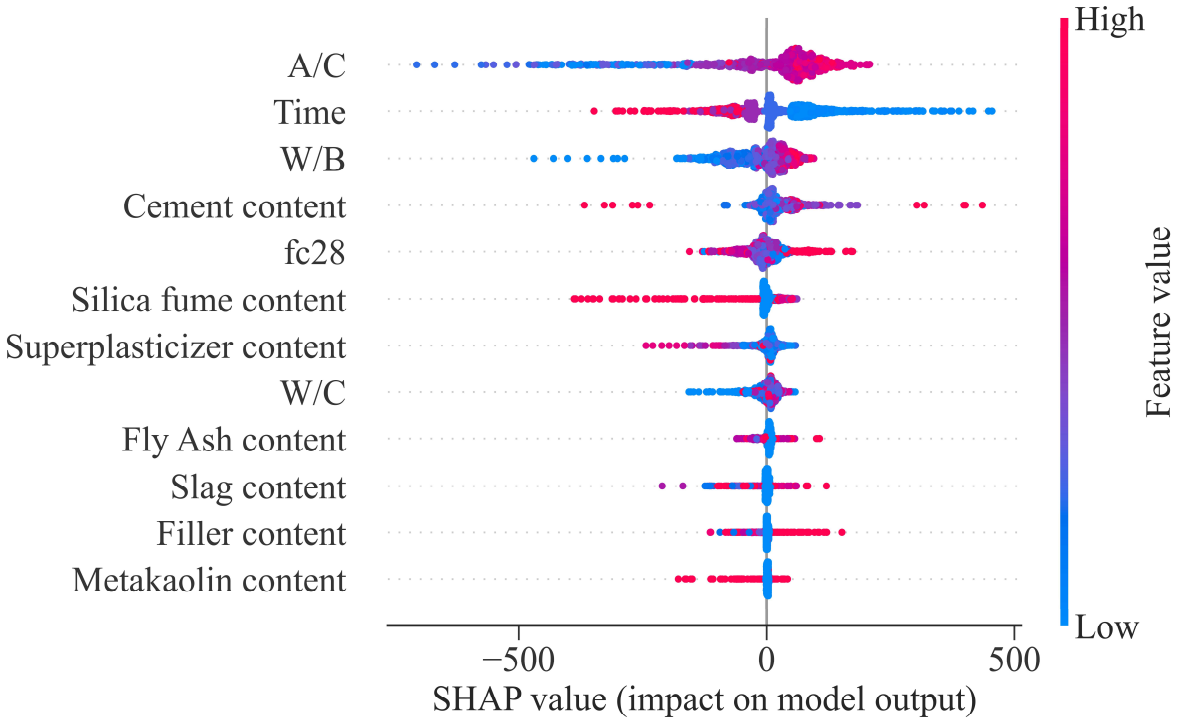

Fig. 8. Global SHAP values of the tuned XGB model

Based on Fig. 9 c), it can be seen that the increasing strength values up to around 100MPa negatively influence SHAP values, which means that transitioning from normal strength to high strength concrete leads to more autogenous shrinkage, independently from the other parameters such as the W/B ratio. Conversely, SHAP values increase for strength higher than around 100MPa up to final values around 140 με, which means that autogenous shrinkage for this type of high performance and ultra-high performance concrete would have been more pronounced if their strength had been smaller. This novel insight might correlate to the quick strength and Young's modulus increase of these concretes, limiting early age autogenous shrinkage.

451 The influence of silica fume can be analyzed using Fig. 9 d). Based on this figure, it can be
452 observed that increasing silica fume values, from 0% to 50% cement replacement, largely
453 decreases SHAP values. However, a spread should be noticed when the silica fume replacement
454 ratio is larger than 20%, and it should be noticed that a 50% replacement ratio can influence SHAP
455 values less than a 20% replacement ratio in the case of some concretes. Therefore, although silica
456 fume is known to increase considerably autogenous shrinkage, novel routes might be found to limit
457 its influence. The other supplementary cementitious materials have a smaller influence on SHAP
458 values. As illustrated in Fig. 9 e), fly ash influence on SHAP values becomes visible on this feature
459 dependence plot for replacement ratios higher than 50%. In this case, cement substitution by fly
460 ash leads to smaller autogenous shrinkage values explained by the slower hydration. Based on Fig.
461 9 f), it can be observed that slag influence on SHAP values is relatively limited as most of the
462 values belong to the [-100 με, 50 με] interval. However, it is worth noting that, according to this
463 detailed analysis, slag negatively influences shrinkage for all the substitution ratios smaller than
464 around 50%, which agrees with the literature [19,74]. On the opposite, different behaviors can be
465 observed for replacement ratios higher than 50%: slag can positively affect shrinkage sometimes,
466 while it still negatively influences shrinkage for other concrete mixes. It can be hypothesized that
467 two competing interests are at stake: the refined pore structures that increase shrinkage and the
468 slower hydration that decrease shrinkage at a given time. As illustrated in Fig. 9 g), filler globally
469 slightly increases shrinkage for substitution rates smaller than 25%, which can be explained by the
470 increased hydration speed. However, substitution ratios higher than 25% systematically positively
471 influence SHAP values, highlighting the restraining effect of filler on the autogenous shrinkage.

472 Finally, though the effect of calcined clay is relatively small according to the model, it can be
473 observed that calcined clay does not influence SHAP values a lot for replacement ratios smaller
474 than 20%, while increasing the substitution rate, the SHAP values decrease. This observation
475 agrees with the literature [24,58]. To conclude, since SHAP gives the influence rules of the
476 different features on the autogenous shrinkage predictions of the model, it can be used to provide
477 novel insights into the shrinkage phenomenon.
478

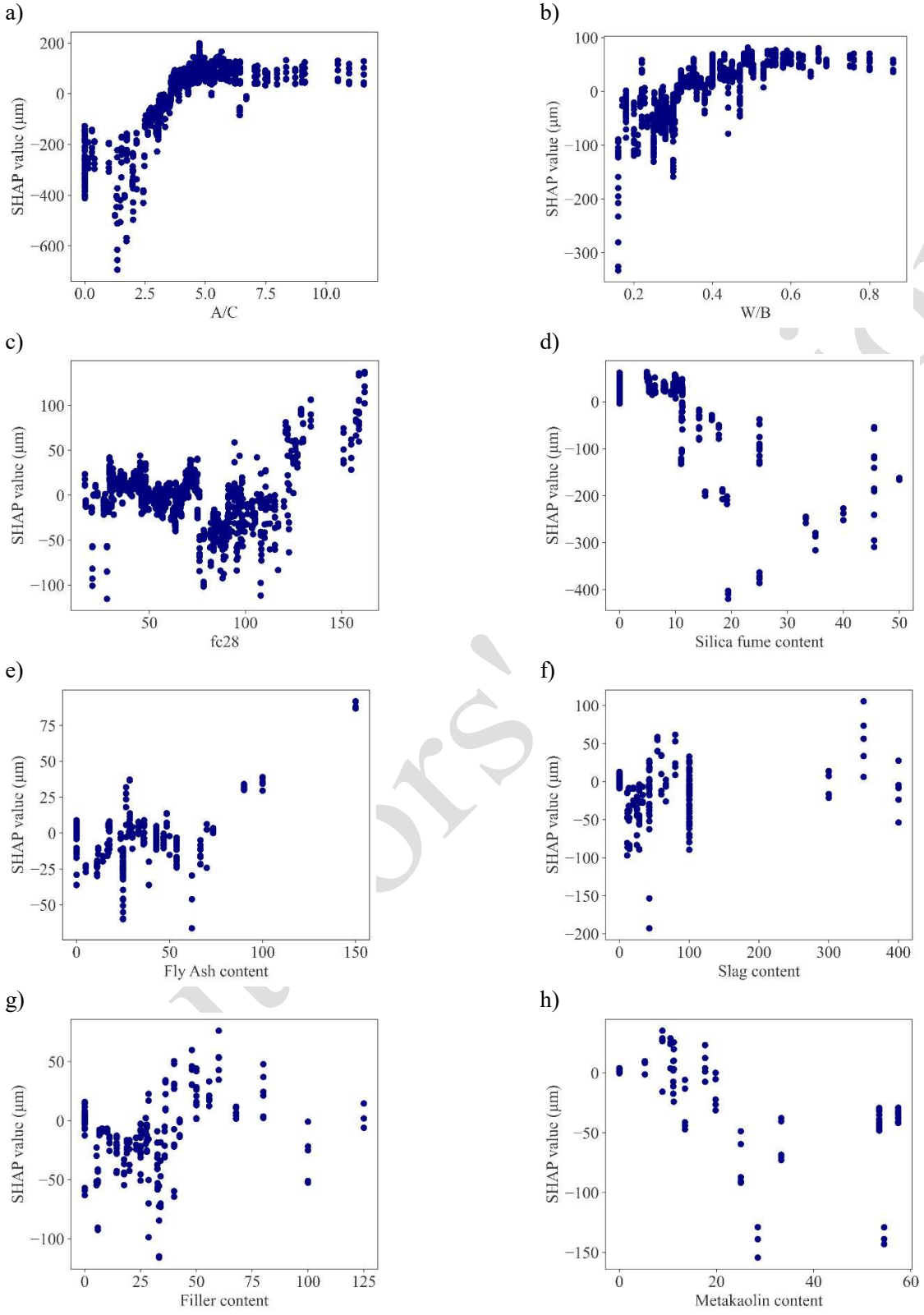

479 **Fig. 9.** Feature dependence plots associated with SHAP for the influential features: a) A/C, b)
480 W/B, c) fc28, d) silica fume, e) fly ash, f) slag, g) filler, and h) calcined clay.

4.3.2 Local interpretation

Besides global interpretations, SHAP also provides useful information to explain the model predictions on individual samples as SHAP decomposes the final prediction into a sum of contributions by all the input variables. Various 28d autogenous shrinkage predictions were thus analyzed for several unknown concrete samples containing various types of SCM. Fig. 10 illustrates explanations for four typical samples.

As shown in Fig. 10 a), the base prediction on the entire set is -229 με. For this sample, the most significant reason for the final autogenous shrinkage prediction of -76 με is the A/C ratio, whose individual contribution amounts to +152 με, meaning this value decreases shrinkage compared to lower A/C ratios. Then time negatively influences the autogenous shrinkage prediction, which can be explained by the fact that 28 days is the final prediction associated with larger shrinkage deformations. The water to binder ratio is the third most influential parameter, as expected based on the global interpretation.

For concrete incorporating silica fume, its relative influence on the outputs can be quantified as illustrated in Fig. 10 b). The presence of silica fume can considerably influence the model prediction. Indeed, as illustrated in the figure, silica fume content becomes the most influential parameter, and, at 28 days, the SHAP value associated to silica fume is around -160 με.

In most analyses, small replacement ratios of other SCM were found only slightly to affect shrinkage values as the A/C and the W/B ratios predominantly influenced the latter, as illustrated in Fig. 10 c) represents the inputs contributions on the autogenous shrinkage prediction of a concrete sample incorporating fly ash with the mass of fly ash equal to 11.1% of the one of cement. However, when larger proportions of cement are replaced, the influence of the SCM can become predominant. Indeed, as illustrated in Fig. 10 d), when half of the cement is replaced by slag, this slag proportion increases shrinkage by around 52 με according to the model.

a)

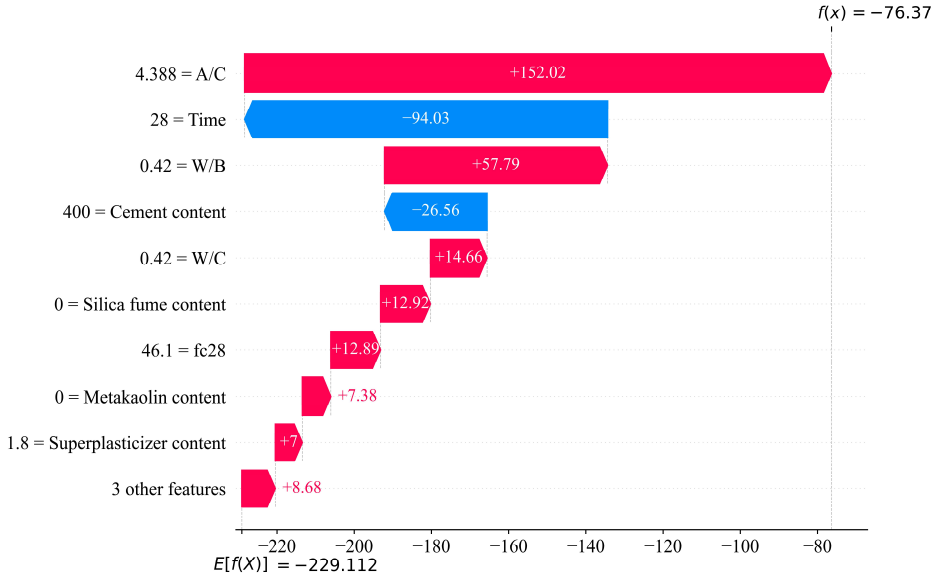
f(x) = −76.37
4.388 = A/C
28 = Time
0.42 = W/B
400 = Cement content
0.42 = W/C
0 = Silica fume content
46.1 = fc28
0 = Metakaolin content
1.8 = Superplasticizer content
3 other features
+152.02
−94.03
+57.79
−26.56
+14.66
+12.92
+12.89
+7.38
+7
+8.68
−220
−200
−180
−160
−140
−120
−100
−80
E[f(X)] = −229.112

b)

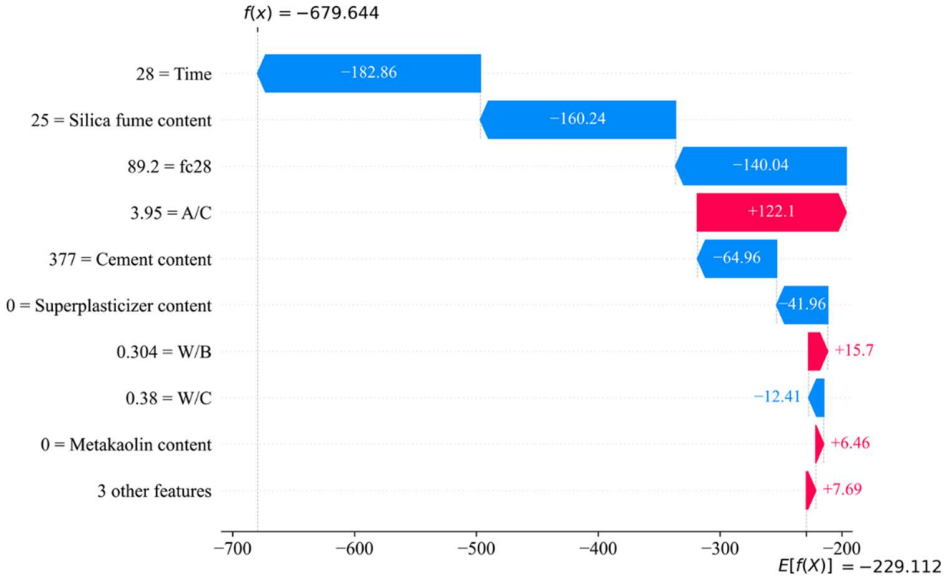
f(x) = −679.644
28 = Time
25 = Silica fume content
89.2 = fc28
3.95 = A/C
377 = Cement content
0 = Superplasticizer content
0.304 = W/B
0.38 = W/C
0 = Metakaolin content
3 other features
−182.86
−160.24
−140.04
+122.1
−64.96
−41.96
+15.7
−12.41
+6.46
+7.69
−700
−600
−500
−400
−300
−200
E[f(X)] = −229.112

c)

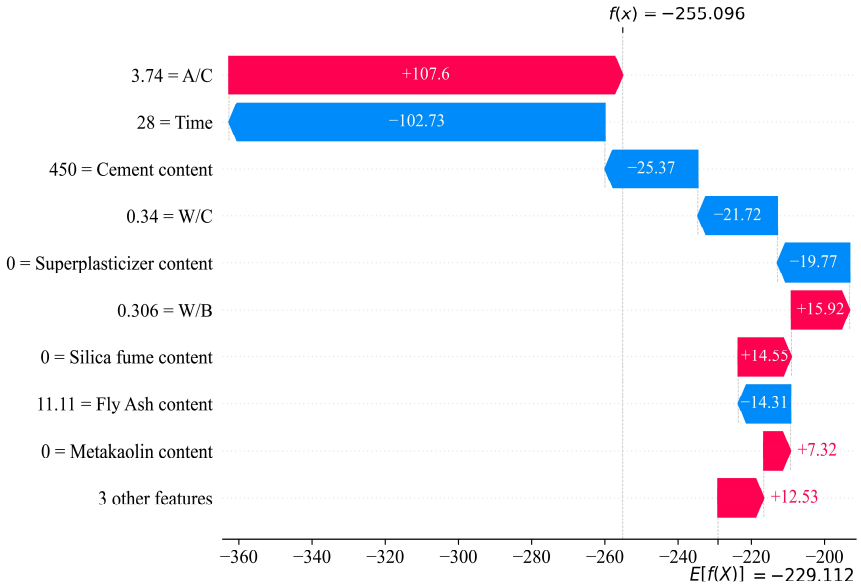

d)

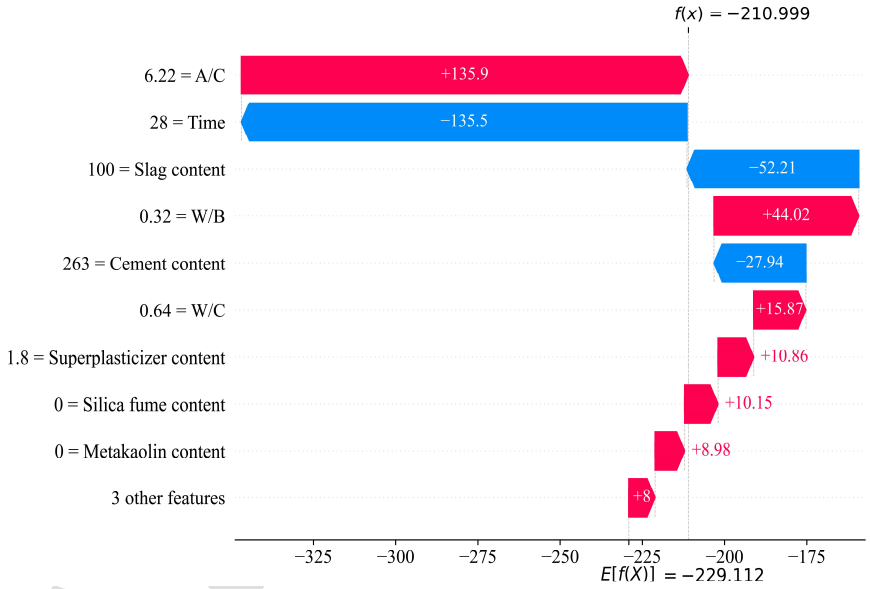

Fig. 10. Local interpretation using SHAP of some of the XGB model autogenous shrinkage predictions: a) normal strength concrete without SCM, b) high strength concrete with silica fume, c) normal strength concrete with fly ash, d) high-strength concrete with 50% of cement replaced by slag.

4.4 Comparison with B4 and CEB analytical models

The developed XGBoost model, the modified B4 and B4s, the CEB MC10, and the CEB MC

10 model's modified version can be compared globally using their respective predictions on the test set composed of unknown concrete formulations. The performance of these four models has been compared with the observed shrinkage values, as illustrated in Fig. 11. It can be observed that, overall, the distribution of the shrinkage values predicted by the developed XGB model is in close agreement with the observed distribution, and the box plots are very similar. Indeed, interquantiles ranges and outliers present similar patterns. The XGB model slightly overestimates the overall shrinkage values, which is good regarding safety issues. Last but not least, the XGB model can predict small swelling values that might occur at an early age, while analytical models cannot be captured correctly this trend.

The analytical models' performance considerably varies. Based on the overall distribution of the shrinkage values, the modified B4 model provides a distribution of the predictions that is in good agreement with the observed distribution. However, one can observe that the mean shrinkage value predicted by the modified B4 model slightly underestimates the observed shrinkage distribution, which might represent a risk regarding safety. The same conclusion applies to the modified version of the B4 S model. Moreover, the predictions made by this model cannot capture the experimental variability, probably due to its simplicity. CEB MC 10 model results clearly underestimate shrinkage, and the size of the overall distribution is considerably smaller than the observed distribution, highlighting the shortcomings of this analytical model. The modified version of the CEB MC 10 model performed better, and the overall distribution of the shrinkage values looks like the observed distribution as the interquartile range is close to the experimental one. However, an apparent overestimation of the shrinkage values and a disability to predict large shrinkage values can be noticed.

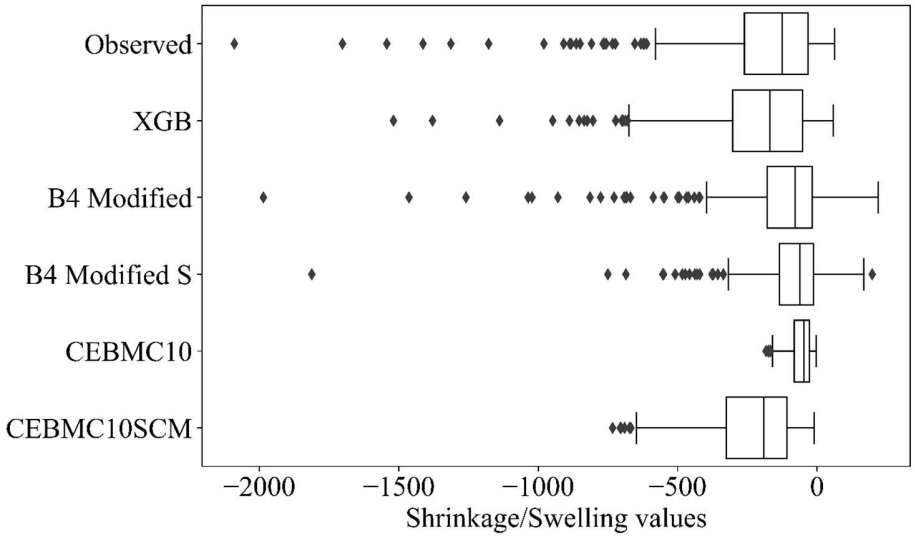

Fig. 11. Box plots of the shrinkage/swelling values predicted by the XGB model compared to the analytical models and the observed values

The model results and the test data can be further compared using the Taylor diagram (Fig. 12), which summarizes three valuable characteristics of the models compared to the measured values: the standard deviation associated with the model's predictions, the correlation between the predictions and the experimental values, and the centered root-mean-square (RMS) difference. As mentioned in the previous paragraph, the standard deviation of the simulated patterns reported on the X-axis largely differs between the models. The standard deviation of the experimental data is almost reproduced by the XGB and the modified version of the B4 model. Indeed, the standard deviations associated with these models are higher than 200 με, close to the 250 με experimental value. Then, the modified B4 S and modified version of the CEB MC 10 model exhibit a standard deviation of around 150 με, which is in relatively good agreement with the observed values. Last, the standard deviation of the classic CEB Model 10 is smaller than 40 με, clearly underestimating the experimental variation and highlighting the model's shortcomings in predicting shrinkage of concrete incorporating SCM. Concerning the correlation of the models with the experimental values, the best correlation is obtained by the XGB model (0.82). This correlation is largely higher than the second-best correlation obtained by the modified B4 model (0.58). The correlation of the modified B4 S model follows. The CEB MC 10 and the modified version of the CEB MC 10 model exhibit correlations close to 0.3-0.4, which is relatively small. Finally, the RMS value of the XGB

model (around 160 με) is clearly better than the ones of the other models, which are higher than 200 με. For all these reasons, it can be concluded that the optimized XGB model significantly outperforms the best analytical models that have been proposed up to date.

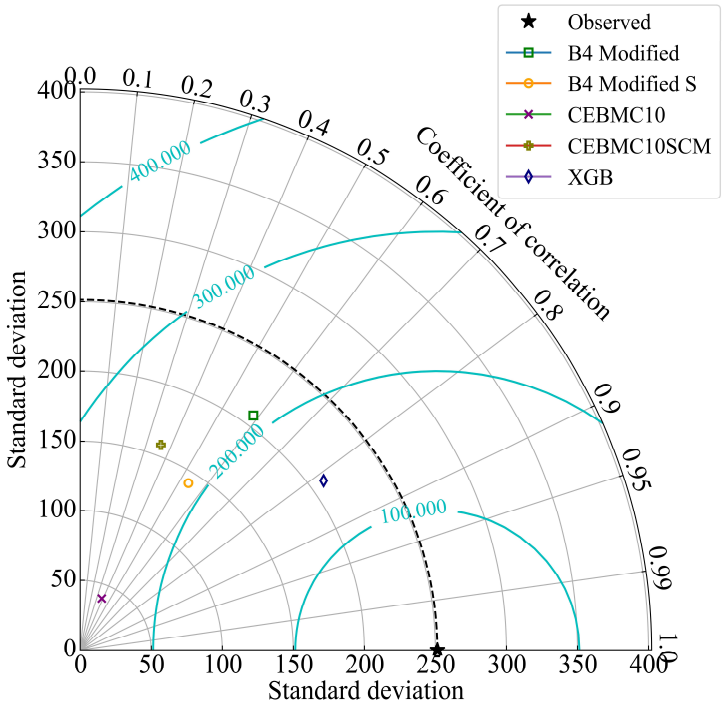

Fig. 12. Taylor diagram representing XGB, B4 and B4s modified, CEB MC 10 and CEB MC 10 modified version models performance.

Based on the XGB model, the autogenous shrinkage predictions of the eight concrete compositions containing various types of SCM have been compared to the analytical models' predictions, as shown in Fig. 13. The detailed formulations are given in Table 4. As illustrated in these figures, the prediction accuracy of the XGB model globally outperforms that of the analytical models in most cases which agrees with Taylor's analysis.

574 **Table 4.** Mortar and concrete compositions of some typical test samples.

Ref	C1	C2	C3	C4	C5	C6	C7	C8
W/C	0.42	0.38	0.34	0.64	0.29	0.43	0.31	0.44
W/B	0.42	0.304	0.306	0.32	0.28	0.3	0.21	0.3
A/C	4.39	3.95	3.74	6.22	4.21	3.68	3.94	3.74
Cement (kg/m^3)	400	377	450	263	428	408	497	416
Silica fume (%)	-	25	-	-	-	14.2	10	-
Fly Ash (%)	-	-	11.1	-	-	28.7	-	-
Slag (%)	-	-	-	100	-	-	-	-
Metakaolin (%)	-	-	-	-	5.3	-	-	10.5
Filler (%)	-	-	-	-	-	-	34	36.2
Sp (%)	1.8	-	-	1.8	3.1	2.1	2.07	1.46
fc28 (MPa)	46.1	89.2	53.4	66.7	91.5	69.7	93	84
Time (days)	1-28	1-28	1-28	1-28	1-28	1-28	1-28	1-28

575

576 In the case of a normal strength concrete with a water-to-binder ratio of 0.42 and without any
577 SCM, the model's prediction agrees with the experimental values, and only a 20 με difference is
578 obtained after 28 days, as illustrated in Fig. 13 a). However, the B4 model better predicted the
579 long-term 28-d shrinkage value. The CEB MC 10 model's modified version largely overestimated
580 the autogenous shrinkage values. On the opposite, as observed in the global statistics, the CEB
581 MC 10 model underestimates the autogenous shrinkage at 28 days.

582 The effect of the cement substitution by silica fume is illustrated in Fig. 13 b). Both the XGB
583 model and the modified version of the CEB MC 10 model can provide good predictions, while the
584 modified versions of the B4 model largely underestimate autogenous shrinkage by around 300 με
585 and the CEB MC 10 model underestimates the shrinkage value by approximately 400 με .

586 As illustrated in Fig. 13 c), the XGB model prediction of the shrinkage values of concrete with
587 a relatively low W/B around 0.3 incorporating fly ash closely matches the experimental values,
588 even at an early age. The analytical models' predictions are relatively far from the experimental
589 values at an early age, which might be attributed to these models' absent or relatively recent
590 considerations of fly ash effects. It should be noticed that the 28d shrinkage values predicted by
591 the modified versions of the B4 and CEB MC10 model are in relatively good agreement with the
592 experimental values, but their prediction might deviate from the measured values for more
593 extended periods.

594 Fig. 13 d) displays the autogenous shrinkage predictions of the models in the case of high-

strength concrete, with a water-to-binder ratio of 0.32, in which 50% of cement has been replaced by slag. In this case, exemplifying modern concretes with high substitution rates, the XGB model also performed well, though slightly underestimating the 28d autogenous shrinkage value. The modified B4 model provides the best prediction, but the modified version of the B4 S model underestimated the shrinkage values as well. The CEB MC 10 models underestimated the shrinkage values, while the modified version of the CEB MC 10 whose prediction can be qualified as correct, still overestimated the shrinkage value by around 75 με. It would be interesting to combine analytical and machine learning models in such a case.

Though more experimental data is needed regarding the influence of calcined clay on drying and autogenous shrinkage, the developed XGB model showed better results than the analytical models in predicting the autogenous shrinkage evolution of concrete mixes incorporating calcined clay, as illustrated in Fig. 13 e). The analytical models which do not consider the effect of calcined clay - modified B4, modified B4 S and CEB MC 10 models - largely underestimated the shrinkage values, while the modified version of the CEB MC 10 models overestimated its influence.

The prediction quality of the models can also be calculated in the case of ternary cement blends. As illustrated in Fig. 13 f), the XGB model captured the combined effect of silica fume and fly ash satisfactorily, as the 28d autogenous shrinkage prediction differs by around 60 με from the experimental value, but overestimates early age shrinkage. In this case, the modified version of the B4 model outputs good yet slightly underestimated results. However, the prediction of the autogenous shrinkage of some ternary formulations might be improved in the future. As illustrated in concrete in Fig. 13 g), the XGB and analytical models predictions are pretty far from the measured values for concrete in which cement is partially substituted by silica fume and filler. In this particular case, the modified version of the CEB MC 10 model provided the best estimation of the final 28-day shrinkage value.

The XGB model's predictions are better in the case of LC^3 concrete incorporating calcined clay and filler, as illustrated in Fig. 13 h) since several formulations of this type are present in the database. In that case, the model predictions are good, especially after 10 days, while the early shrinkage values are overestimated. Other models cannot capture the experimental shrinkage evolution.

a)

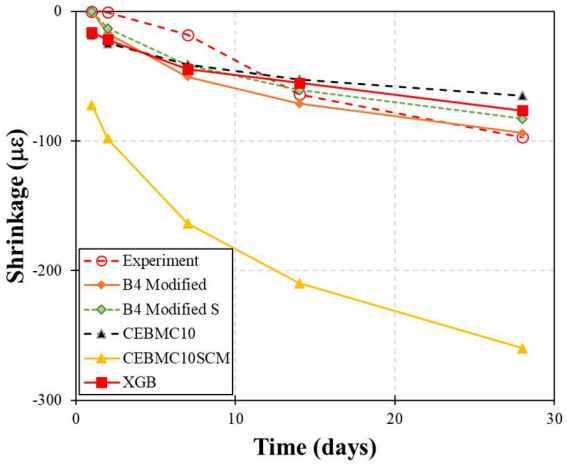

b)

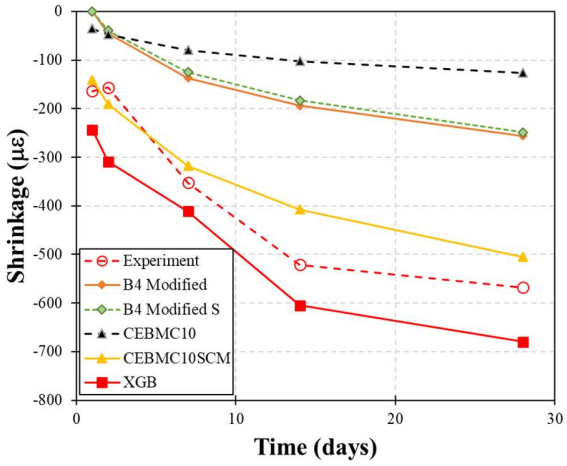

c)

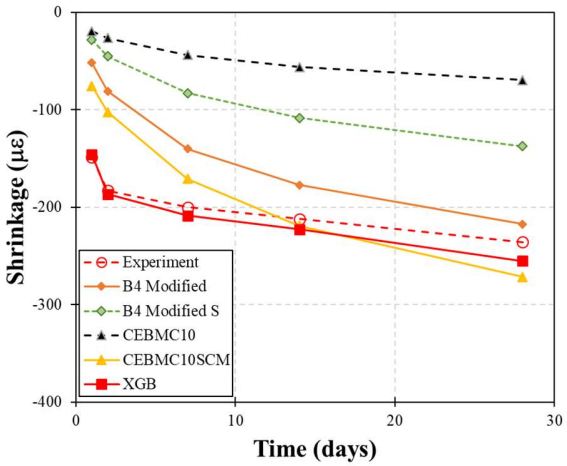

d)

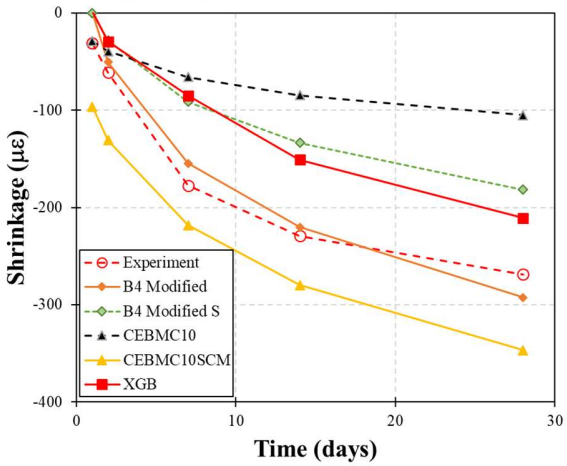

e)

f)

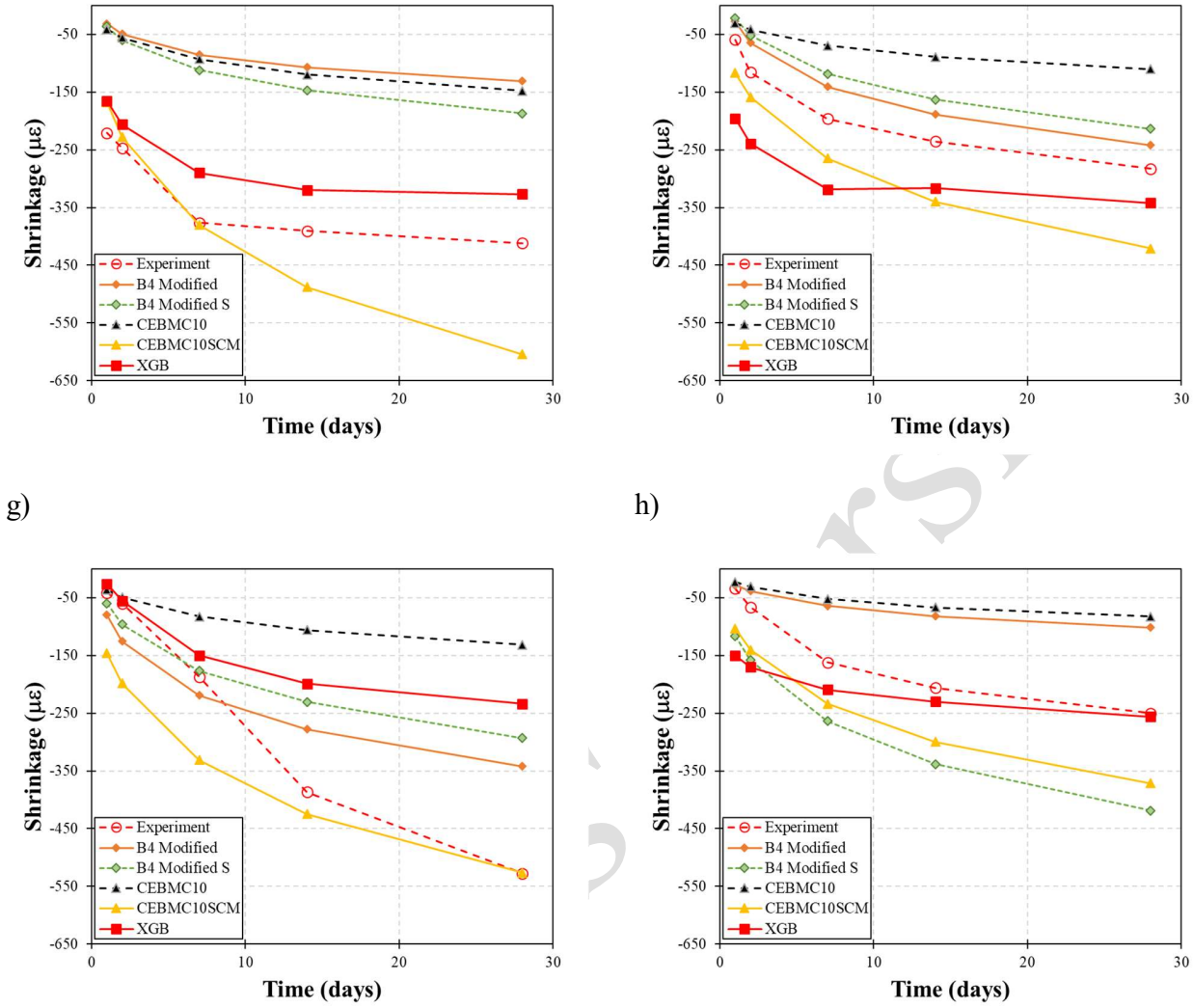

Fig. 13. Comparison of the autogenous shrinkage predictions of the XGB model and the analytical models for several unknown concrete formulations detailed in Table 4: a) normal strength concrete without SCM, b) high strength concrete with silica fume, c) normal strength concrete with fly ash, d) high-strength concrete with 50% of cement replaced by slag, e) high-strength concrete incorporating calcined clay, f) high-strength concrete with cement replaced by silica fume and fly ash, g) high-strength concrete with silica fume and filler, h) normal strength concrete incorporating calcined clay and filler (LC^3 concrete).

4.5 Web application

A web application has been built using the first model trained on the whole database to provide autogenous shrinkage predictions of various concrete formulations. The user can input the concrete

formulation using several sliders whose minimum and maximum values corresponds to the ones from the database, and then predictions of the shrinkage values at 1 day, 2 days, 7 days, 14 days and 28 days are computed online based on the model developed in this study. Default values corresponding to a high-strength concrete formulation incorporating silica fume are considered from a study not included in the database [75]. A graph is plotted to visualize the predictions as illustrated in Fig.14. The web application is available at https://share.streamlit.io/bhilloul/concrete-auto-shrinkage-ai-streamlit/main .

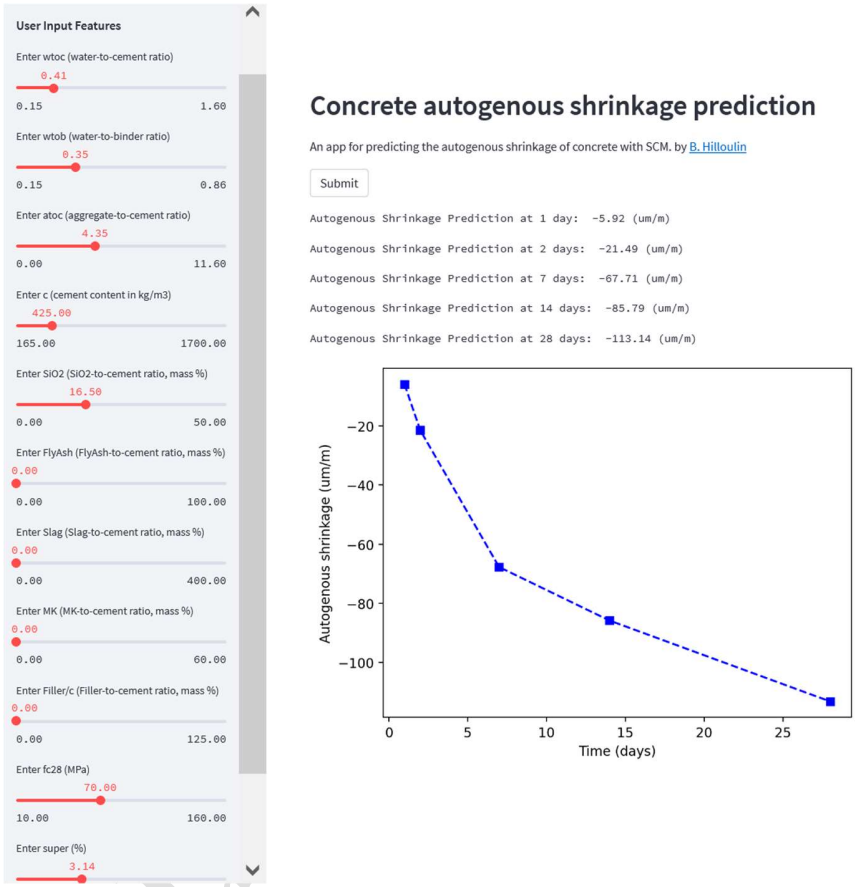

Fig. 14. Web application for autogenous shrinkage prediction of concrete incorporating SCM.

5 Conclusions

This study examined the usage and potential of several Machine Learning (ML) algorithms to precisely predict the autogenous shrinkage of low-carbon cementitious materials with various types of supplementary cementitious materials (SCM) and compared the results with analytical models, e.g., the modified version of the B4 and B4 S models, the CEB MC 10, and the CEB MC

10 modified version. To this end, an extensive database of autogenous shrinkage measurements has been built based on a previous study. First, Gradient Boosting (GB), XG Boost (XGB), Support Vector Machine (SVM), and an Artificial Neural Network (ANN) model have been optimized using grid search hyperparameter optimization, and their performance has been assessed using k-fold cross-validation. The best model has been further analyzed using the Shapley Additives Explanations (SHAP) to facilitate interpretations and provide novel insights into the autogenous shrinkage mechanism. Finally, the developed model has been compared to the aforementioned analytical models, some recently adapted to consider the effect of SCM. Based on the results, the following main conclusions can be drawn:

- An extensive database composed of 1482 autogenous shrinkage curves of various binary, ternary and quaternary cement paste, mortar, and concrete incorporating silica fume, fly ash, slag, calcined clay, and filler, containing also concrete 28-day compressive strength, has been built using data from the literature.
- ML models can accurately predict the autogenous shrinkage, and their hyperparameters can be optimized through grid search. Indeed, R^2 values of around 0.805 to 0.931 have been obtained on the test set. The best model identified in this study is XGB.
- The relative influence of the model inputs on the predictions can be analyzed using SHAP values. Global SHAP values agreed with the experimental observations, and the A/C ratio, time, W/B ratio, and silica fume content are particularly impacting. Local SHAP analysis helped identify some evolutions of the shrinkage behavior with increasing amounts of SCM, for example, the competition between the shrinkage increase due to the pore refinement and the shrinkage delay due to slower hydration.
- The model predictions of completely unknown shrinkage behavior of concretes incorporating SCM are significantly better than the predictions of analytical models such as the modified B4 models, the CEB MC 10, and the modified version CEB MC 10, even though some analytical models can perform better predictions for specific formulations. Detailed comparisons of the models' shrinkage predictions of various concrete compositions have been studied thoroughly.
- A web application has been developed to provide fast and precise predictions to the

scientific and industrial community and drive further low-carbon cementitious materials developments.

The study might open up novel research and industrial perspectives on shrinkage prediction of eco-friendly cementitious materials using advanced Machine Learning techniques.

CRediT authorship contribution statement

Benoit Hilloulin: Conceptualization, Methodology, Investigation, Software, Formal analysis, Writing - original draft, Writing - review & editing, Validation.

Van Quan Tran: Conceptualization, Methodology, Software**,** Visualization**.** Writing -original draft, Writing - review & editing.

Conflict of Interest: The authors declare that there is no conflict of interest.

Funding: This research did not receive any specific grant from funding agencies in the public, commercial, or not-for-profit sectors.

References

[1] S.A. Moghaddas, M. Nekoei, E. Mohammadi Golafshani, M. Nehdi, M. Arashpour, Modeling carbonation depth of recycled aggregate concrete using novel automatic regression technique, Journal of Cleaner Production. (2022) 133522. https://doi.org/10.1016/j.jclepro.2022.133522.

[2] D.N. Huntzinger, T.D. Eatmon, A life-cycle assessment of Portland cement manufacturing: comparing the traditional process with alternative technologies, Journal of Cleaner Production. 17 (2009) 668–675. https://doi.org/10.1016/j.jclepro.2008.04.007.

[3] B. Lothenbach, K. Scrivener, R.D. Hooton, Supplementary cementitious materials, Cement and Concrete Research. 41 (2011) 1244–1256. https://doi.org/10.1016/j.cemconres.2010.12.001.

[4] J. de Brito, R. Kurda, The past and future of sustainable concrete: A critical review and new strategies on cement-based materials, Journal of Cleaner Production. 281 (2021) 123558. https://doi.org/10.1016/j.jclepro.2020.123558.

[5] L. Wu, N. Farzadnia, C. Shi, Z. Zhang, H. Wang, Autogenous shrinkage of high performance concrete: A review, Construction and Building Materials. 149 (2017) 62–75. https://doi.org/10.1016/j.conbuildmat.2017.05.064.

[6] E. Tazawa, S. Miyazawa, Experimental study on mechanism of autogenous shrinkage of concrete, Cement and Concrete Research. 25 (1995) 1633–1638. https://doi.org/10.1016/0008-8846(95)00159-X.

[7] O. Bernard, E. Brühwiler, Influence of autogenous shrinkage on early age behaviour of structural elements consisting of concretes of different ages, Materials and Structures. 35 (2002) 7. https://doi.org/10.1007/BF02483123.

[8] J. Kheir, A. Klausen, T.A. Hammer, L. De Meyst, B. Hilloulin, K. Van Tittelboom, A. Loukili, N. De Belie, Early age autogenous shrinkage cracking risk of an ultra-high performance concrete (UHPC) wall: Modelling and experimental results, Engineering Fracture Mechanics. 257 (2021) 108024.

https://doi.org/10.1016/j.engfracmech.2021.108024.
[9] International Federation for Structural Concrete, fib Model Code for Concrete Structures, Lausanne, Switzerland, 2010.
[10] RILEM Technical Committee TC-242-MDC (Zdeněk P. Bažant, chair), RILEM draft recommendation: TC-242-MDC multi-decade creep and shrinkage of concrete: material model and structural analysis*: Model B4 for creep, drying shrinkage and autogenous shrinkage of normal and high-strength concretes with multi-decade applicability, Mater Struct. 48 (2015) 753–770. https://doi.org/10.1617/s11527-014-0485-2.
[11] M.H. Hubler, R. Wendner, Z.P. Bažant, Statistical justification of Model B4 for drying and autogenous shrinkage of concrete and comparisons to other models, Mater Struct. 48 (2015) 797–814. https://doi.org/10.1617/s11527-014-0516-z.
[12] EN 2004, ed., General rules and rules for building, Eurocode 2 –Design of concrete structures, Part 1, n.d.
[13] American Concrete Institute, ACI Committee 209--Creep and Shrinkage, eds., Guide for modeling and calculating shrinkage and creep in hardened concrete, American Concrete Institute, Farmington Hills, MI, 2008.
[14] M. Rasoolinejad, Prediction of autogenous shrinkage in concrete from material composition or strength calibrated by a large database, as update to model B4, Materials and Structures. (2019) 17.
[15] J.-R. Weng, W.-C. Liao, Microstructure and shrinkage behavior of high-performance concrete containing supplementary cementitious materials, Construction and Building Materials. 308 (2021) 125045. https://doi.org/10.1016/j.conbuildmat.2021.125045.
[16] C. Youssef Namnoum, B. Hilloulin, F. Grondin, A. Loukili, Determination of the origin of the strength regain after self-healing of binary and ternary cementitious materials including slag and metakaolin, Journal of Building Engineering. 41 (2021) 102739. https://doi.org/10.1016/j.jobe.2021.102739.
[17] P. Termkhajornkit, T. Nawa, M. Nakai, T. Saito, Effect of fly ash on autogenous shrinkage, Cement and Concrete Research. 35 (2005) 473–482. https://doi.org/10.1016/j.cemconres.2004.07.010.
[18] J.M. Khatib, Performance of self-compacting concrete containing fly ash, Construction and Building Materials. 22 (2008) 1963–1971. https://doi.org/10.1016/j.conbuildmat.2007.07.011.
[19] K.M. Lee, H.K. Lee, S.H. Lee, G.Y. Kim, Autogenous shrinkage of concrete containing granulated blast-furnace slag, Cement and Concrete Research. 36 (2006) 1279–1285. https://doi.org/10.1016/j.cemconres.2006.01.005.
[20] A. Itim, K. Ezziane, E.-H. Kadri, Compressive strength and shrinkage of mortar containing various amounts of mineral additions, Construction and Building Materials. 25 (2011) 3603–3609. https://doi.org/10.1016/j.conbuildmat.2011.03.055.
[21] M. Bouasker, N.E.H. Khalifa, P. Mounanga, N. Ben Kahla, Early-age deformation and autogenous cracking risk of slag–limestone filler-cement blended binders, Construction and Building Materials. 55 (2014) 158–167. https://doi.org/10.1016/j.conbuildmat.2014.01.037.
[22] C. Jiang, Y. Yang, Y. Wang, Y. Zhou, C. Ma, Autogenous shrinkage of high performance concrete containing mineral admixtures under different curing temperatures, Construction and Building Materials. 61 (2014) 260–269. https://doi.org/10.1016/j.conbuildmat.2014.03.023.
[23] K. Scrivener, F. Martirena, S. Bishnoi, S. Maity, Calcined clay limestone cements (LC3), Cement and Concrete Research. 114 (2018) 49–56. https://doi.org/10.1016/j.cemconres.2017.08.017.
[24] P.J.P. Gleize, M. Cyr, G. Escadeillas, Effects of metakaolin on autogenous shrinkage of cement pastes, Cement and Concrete Composites. 29 (2007) 80–87. https://doi.org/10.1016/j.cemconcomp.2006.09.005.
[25] Y. Dhandapani, T. Sakthivel, M. Santhanam, R. Gettu, R.G. Pillai, Mechanical properties and durability performance of concretes with Limestone Calcined Clay Cement (LC3), Cement and Concrete Research. 107 (2018) 136–151. https://doi.org/10.1016/j.cemconres.2018.02.005.
[26] Q.D. Nguyen, S. Afroz, Y. Zhang, T. Kim, W. Li, A. Castel, Autogenous and total shrinkage of limestone calcined clay cement (LC3) concretes, Construction and Building Materials. 314 (2022) 125720. https://doi.org/10.1016/j.conbuildmat.2021.125720.
[27] M. Valcuende, E. Marco, C. Parra, P. Serna, Influence of limestone filler and viscosity-modifying admixture on the shrinkage of self-compacting concrete, Cement and Concrete Research. 42 (2012) 583–592. https://doi.org/10.1016/j.cemconres.2012.01.001.
[28] A. Alrifai, S. Aggoun, A. Kadri, S. Kenai, E. Kadri, Paste and mortar studies on the influence of mix design

771 parameters on autogenous shrinkage of self-compacting concrete, Construction and Building Materials. 47
772 (2013) 969–976. https://doi.org/10.1016/j.conbuildmat.2013.05.024.
773 [29] B. Craeye, G. De Schutter, B. Desmet, J. Vantomme, G. Heirman, L. Vandewalle, Ö. Cizer, S. Aggoun, E.H.
774 Kadri, Effect of mineral filler type on autogenous shrinkage of self-compacting concrete, Cement and
775 Concrete Research. 40 (2010) 908–913. https://doi.org/10.1016/j.cemconres.2010.01.014.
776 [30] T. Sakthivel, R. Gettu, R. Pillai, ADJUSTMENT OF RILEM B4 MODEL PARAMETERS FOR BETTER
777 PREDICTION OF THE SHRINKAGE RESPONSE OF BLENDED CEMENT CONCRETE, Indian
778 Concrete Journal. 95 (2021) 51–57.
779 [31] Z. Li, J. Yoon, R. Zhang, F. Rajabipour, W.V. Srubar III, I. Dabo, A. Radlińska, Machine learning in
780 concrete science: applications, challenges, and best practices, Npj Comput Mater. 8 (2022) 127.
781 https://doi.org/10.1038/s41524-022-00810-x.
782 [32] I.-C. Yeh, Modeling of strength of high-performance concrete using artificial neural networks, Cement and
783 Concrete Research. 28 (1998) 1797–1808. https://doi.org/10.1016/S0008-8846(98)00165-3.
784 [33] J.-S. Chou, C.-F. Tsai, A.-D. Pham, Y.-H. Lu, Machine learning in concrete strength simulations: Multi-
785 nation data analytics, Construction and Building Materials. 73 (2014) 771–780.
786 https://doi.org/10.1016/j.conbuildmat.2014.09.054.
787 [34] D.K. Bui, T. Nguyen, J.S. Chou, H. Nguyen-Xuan, T.D. Ngo, A modified firefly algorithm-artificial neural
788 network expert system for predicting compressive and tensile strength of high-performance concrete,
789 Construction and Building Materials. 180 (2018) 320–333.
790 https://doi.org/10.1016/j.conbuildmat.2018.05.201.
791 [35] M.J. Munir, S.M. Saleem Kazmi, Y.-F. Wu, X. Lin, M.R. Ahmad, Development of a novel compressive
792 strength design equation for natural and recycled aggregate concrete through advanced computational
793 modeling, Journal of Building Engineering. (2022) 104690. https://doi.org/10.1016/j.jobe.2022.104690.
794 [36] H.S. Ullah, R.A. Khushnood, J. Ahmad, F. Farooq, Predictive modelling of sustainable lightweight foamed
795 concrete using machine learning novel approach, Journal of Building Engineering. 56 (2022) 104746.
796 https://doi.org/10.1016/j.jobe.2022.104746.
797 [37] W.E. Elemam, A.H. Abdelraheem, M.G. Mahdy, A.M. Tahwia, Optimizing fresh properties and compressive
798 strength of self-consolidating concrete, Construction and Building Materials. 249 (2020) 118781.
799 https://doi.org/10.1016/j.conbuildmat.2020.118781.
800 [38] J. Karthikeyan, A. Upadhyay, N.M. Bhandari, Artificial Neural Network for Predicting Creep and Shrinkage
801 of High Performance Concrete, ACT. 6 (2008) 135–142. https://doi.org/10.3151/jact.6.135.
802 [39] P. Chen, W. Zheng, Y. Wang, W. Chang, Creep model of high-strength concrete containing supplementary
803 cementitious materials, Construction and Building Materials. 202 (2019) 494–506.
804 https://doi.org/10.1016/j.conbuildmat.2019.01.005.
805 [40] R. Cai, T. Han, W. Liao, J. Huang, D. Li, A. Kumar, H. Ma, Prediction of surface chloride concentration of
806 marine concrete using ensemble machine learning, Cement and Concrete Research. 136 (2020) 106164.
807 https://doi.org/10.1016/j.cemconres.2020.106164.
808 [41] I. Nunez, M.L. Nehdi, Machine learning prediction of carbonation depth in recycled aggregate concrete
809 incorporating SCMs, Construction and Building Materials. 287 (2021) 123027.
810 https://doi.org/10.1016/j.conbuildmat.2021.123027.
811 [42] X. Wu, S. Zheng, Z. Feng, B. Chen, Y. Qin, W. Xu, Y. Liu, Prediction of the frost resistance of high-
812 performance concrete based on RF-REF: A hybrid prediction approach, Construction and Building Materials.
813 333 (2022) 127132. https://doi.org/10.1016/j.conbuildmat.2022.127132.
814 [43] L. Bal, F. Buyle-Bodin, Artificial neural network for predicting drying shrinkage of concrete, Construction
815 and Building Materials. 38 (2013) 248–254. https://doi.org/10.1016/j.conbuildmat.2012.08.043.
816 [44] B. Hilloulin, V.Q. Tran, Using machine learning techniques for predicting autogenous shrinkage of concrete
817 incorporating superabsorbent polymers and supplementary cementitious materials, Journal of Building
818 Engineering. 49 (2022) 104086. https://doi.org/10.1016/j.jobe.2022.104086.
819 [45] B. Hilloulin, M. Robira, A. Loukili, Coupling statistical indentation and microscopy to evaluate
820 micromechanical properties of materials: Application to viscoelastic behavior of irradiated mortars, Cement
821 and Concrete Composites. 94 (2018) 153–165. https://doi.org/10.1016/j.cemconcomp.2018.09.008.
822 [46] B. Hilloulin, M. Lagrange, M. Duvillard, G. Garioud, ε–greedy automated indentation of cementitious

materials for phase mechanical properties determination, Cement and Concrete Composites. (2022) 104465. https://doi.org/10.1016/j.cemconcomp.2022.104465.
[47] B. Hilloulin, I. Bekrine, E. Schmitt, A. Loukili, Open-source deep learning-based air-voids detection algorithm for concrete microscopic images, Journal of Microscopy. (2022) jmi.13098. https://doi.org/10.1111/jmi.13098.
[48] M. Liang, Y. Gan, Z. Chang, Z. Wan, E. Schlangen, B. Šavija, Microstructure-informed deep convolutional neural network for predicting short-term creep modulus of cement paste, Cement and Concrete Research. 152 (2022) 106681. https://doi.org/10.1016/j.cemconres.2021.106681.
[49] P. Teck, R. Snellings, J. Elsen, Method for quantifying the reaction degree of slag in alkali-activated cements using deep learning-based electron microscopy image analysis, Journal of Microscopy. (2022) jmi.13094. https://doi.org/10.1111/jmi.13094.
[50] B. Hilloulin, I. Bekrine, E. Schmitt, A. Loukili, Modular Deep Learning Segmentation Algorithm for Concrete Microscopic Images, Construction and Building Materials. (2022). https://doi.org/10.1016/j.conbuildmat.2022.128736.
[51] R. Zhang, Y. Liu, H. Sun, Physics-guided convolutional neural network (PhyCNN) for data-driven seismic response modeling, Engineering Structures. 215 (2020) 110704. https://doi.org/10.1016/j.engstruct.2020.110704.
[52] B.K. Oh, H.S. Park, B. Glisic, Prediction of long-term strain in concrete structure using convolutional neural networks, air temperature and time stamp of measurements, Automation in Construction. 126 (2021) 103665. https://doi.org/10.1016/j.autcon.2021.103665.
[53] S.M. Lundberg, S.-I. Lee, A Unified Approach to Interpreting Model Predictions, in: Proceedings of the 31st International Conference on Neural Information Processing Systems, Curran Associates Inc., Red Hook, NY, USA, 2017: pp. 4768–4777.
[54] M. Liang, Z. Chang, Z. Wan, Y. Gan, E. Schlangen, B. Šavija, Interpretable Ensemble-Machine-Learning models for predicting creep behavior of concrete, Cement and Concrete Composites. (2021) 104295. https://doi.org/10.1016/j.cemconcomp.2021.104295.
[55] Y. Sun, R. Yu, Z. Shui, X. Wang, D. Qian, B. Rao, J. Huang, Y. He, Understanding the porous aggregates carrier effect on reducing autogenous shrinkage of Ultra-High Performance Concrete (UHPC) based on response surface method, Construction and Building Materials. 222 (2019) 130–141. https://doi.org/10.1016/j.conbuildmat.2019.06.151.
[56] H.K. Lee, K.M. Lee, B.G. Kim, Autogenous shrinkage of high-performance concrete containing fly ash, Magazine of Concrete Research. (2003) 9.
[57] P.Y. Yan, Z.C. Chen, J.C. Wang, F. Zheng, Autogenous shrinkage of concrete prepared with the binders containing different kinds of mineral admixtures, in: ICCC2007, 2007.
[58] J.J. Brooks, M.A.M. Johari, Effect of metakaolin on creep and shrinkage of concrete, Cement and Concrete Composites. (2001) 8.
[59] A. Duran-Herrera, J. De-León-Esquivel, D.P. Bentz, P. Valdez-Tamez, Self-compacting concretes using fly ash and fine limestone powder: Shrinkage and surface electrical resistivity of equivalent mortars, Construction and Building Materials. 199 (2019) 50–62. https://doi.org/10.1016/j.conbuildmat.2018.11.191.
[60] M.-Y. Xuan, Y. Han, X.-Y. Wang, The Hydration, Mechanical, Autogenous Shrinkage, Durability, and Sustainability Properties of Cement–Limestone–Slag Ternary Composites, Sustainability. 13 (2021) 1881. https://doi.org/10.3390/su13041881.
[61] S.M. Lundberg, G. Erion, H. Chen, A. DeGrave, J.M. Prutkin, B. Nair, R. Katz, J. Himmelfarb, N. Bansal, S.-I. Lee, From local explanations to global understanding with explainable AI for trees, Nat Mach Intell. 2 (2020) 56–67. https://doi.org/10.1038/s42256-019-0138-9.
[62] C. Cortes, V. Vapnik, Support-vector networks, Mach Learn. 20 (1995) 273–297. https://doi.org/10.1007/BF00994018.
[63] A.J. Smola, B. Schölkopf, A tutorial on support vector regression, Statistics and Computing. 14 (2004) 199–222. https://doi.org/10.1023/B:STCO.0000035301.49549.88.
[64] D.P. Kingma, J. Ba, Adam: A Method for Stochastic Optimization, arXiv, 2017. https://doi.org/10.48550/arXiv.1412.6980.
[65] M.M. Ahmed, M. Abdel-Aty, Application of Stochastic Gradient Boosting Technique to Enhance Reliability

of Real-Time Risk Assessment: Use of Automatic Vehicle Identification and Remote Traffic Microwave Sensor Data, Transportation Research Record. 2386 (2013) 26–34. https://doi.org/10.3141/2386-04.
[66] J. Friedman, Greedy Function Approximation: A Gradient Boosting Machine, Annals of Statistics. 29 (2001) 1189–1232. https://doi.org/10.2307/2699986.
[67] S. Kirkpatrick, C.D. Gelatt, M.P. Vecchi, Optimization by simulated annealing, Science. 220 (1983) 671–680. https://doi.org/10.1126/science.220.4598.671.
[68] S. Koziel, X.-S. Yang, eds., Computational Optimization, Methods and Algorithms, Springer-Verlag, Berlin Heidelberg, 2011. https://doi.org/10.1007/978-3-642-20859-1.
[69] C.M. Martínez, D. Cao, 2 - Integrated energy management for electrified vehicles, in: C.M. Martínez, D. Cao (Eds.), Ihorizon-Enabled Energy Management for Electrified Vehicles, Butterworth-Heinemann, 2019: pp. 15–75. https://doi.org/10.1016/B978-0-12-815010-8.00002-8.
[70] W. Gao, C. Mi, Hybrid vehicle design using global optimisation algorithms, IJEHV. 1 (2007) 57. https://doi.org/10.1504/IJEHV.2007.014447.
[71] V.Q. Tran, Hybrid gradient boosting with meta-heuristic algorithms prediction of unconfined compressive strength of stabilized soil based on initial soil properties, mix design and effective compaction, Journal of Cleaner Production. (2022) 131683. https://doi.org/10.1016/j.jclepro.2022.131683.
[72] V.Q. Tran, L.Q. Nguyen, Using machine learning technique for designing reinforced lightweight soil, Journal of Intelligent & Fuzzy Systems. 43 (2022) 1633–1650. https://doi.org/10.3233/JIFS-212621.
[73] M. Rasoolinejad, S. Rahimi-Aghdam, Z.P. Bažant, Prediction of autogenous shrinkage in concrete from material composition or strength calibrated by a large database, as update to model B4, Mater Struct. 52 (2019) 33. https://doi.org/10.1617/s11527-019-1331-3.
[74] A. Darquennes, S. Staquet, M.-P. Delplancke-Ogletree, B. Espion, Effect of autogenous deformation on the cracking risk of slag cement concretes, Cement and Concrete Composites. 33 (2011) 368–379. https://doi.org/10.1016/j.cemconcomp.2010.12.003.
[75] M. Mazloom, A.A. Ramezanianpour, J.J. Brooks, Effect of silica fume on mechanical properties of high-strength concrete, Cement and Concrete Composites. 26 (2004) 347–357. https://doi.org/10.1016/S0958-9465(03)00017-9.